Computer simulation of the dynamics of aqueous solvation

Mark Maroncelli and Graham R. Fleming

Citation: The Journal of Chemical Physics **89**, 5044 (1988); doi: 10.1063/1.455649
View online: http://dx.doi.org/10.1063/1.455649
View Table of Contents: http://scitation.aip.org/content/aip/journal/jcp/89/8?ver=pdfcov
Published by the AIP Publishing

Computer simulation of the dynamics of aqueous solvation

Mark Maroncelli
Department of Chemistry, The Pennsylvania State University, 152 Davey Laboratory, University Park, Pennsylvania 16802

Graham R. Fleming
Department of Chemistry and the James Franck Institute, The University of Chicago, Chicago, Illinois 60637

(Received 7 June 1988; accepted 29 June 1988)

Equilibrium and nonequilibrium molecular dynamics computer simulations have been used to study the time dependence of solvation in water. The systems investigated consisted of monatomic ions immersed in large spherical clusters of ST2 water. Relaxation of the solvation energy following step junction jumps in the solute's charge, dipole moment, and quadrupole moment have been determined from equilibrium molecular dynamics (MD) simulations under the assumption of a linear solvation response. The relaxation times observed differ substantially depending on the type of multipole jump and the charge/size ratio of the solute. These results could not be quantitatively understood on the basis either of continuum or molecular theories of solvation dynamics currently available. Even the qualitative picture of a distribution of relaxation times which monatonically increases with distance away from the solute is not correct for the systems studied. This lack of agreement is partially explained in terms of the structured environment of the first solvation shell of aqueous solutes. However, translational mechanisms of polarization decay and effects due to the finite distribution of charge within solvent molecules, which should be operative in less structured solvents as well, also contribute to deviations from theoretical predictions. The validity of a linear response approach has been examined for the case of charge jumps using nonequilibrium simulations. The observed dynamics are not generally independent of the size of the charge jump and thus linear response theories are not strictly applicable. In most cases, however, predictions based on a linear response calculation using the equilibrium dynamics of the appropriate reference system still provide a reasonable description of the actual nonequilibrium dynamics.

I. INTRODUCTION

Solvation and solvent effects are of major importance in many areas of chemistry and their study has long enjoyed a venerable place in chemical research.[1] A question that has only lately come to the forefront in this area is "How fast is solvation?" That is, how long does it take a polar solvent to respond when the electronic makeup of a solute changes? Driving the current interest in this question are recent theories that point to the importance of *dynamical* solvent effects on charge transfer reactions in polar solution.[2–7] The strength of the coupling between a reacting system and its solvent surroundings depends sensitively on the intrinsic rate of reaction compared to the rate at which the solvent can act to stabilize the attendant charge redistributions. While this connection is theoretically well established, our understanding of the dynamical aspects of solvation is far from complete. In the present work we report results of molecular dynamics computer simulations aimed at learning more about this fundamental problem.

The original theoretical treatments describing solvation of newly formed ions or dipoles modeled the solvent in terms of a homogeneous dielectric continuum, completely specified by its experimental dielectric dispersion $\epsilon(\omega)$.[8–12] As in nearly all current models, the solute was viewed as a spherical cavity containing a point charge, point dipole, etc.[13] For the simplest case of a Debye-type $\epsilon(\omega)$, such continuum models predict an exponential relaxation of the solvation energy in response to a change in the solute charge, dipole moment, etc. The response time is approximately equal to the solvent's longitudinal relaxation time τ_L.[14] In polar solvents, the longitudinal relaxation time is typically much shorter than time scales for single-solvent reorientation, reflecting the fact that the solvation response involves the coupled response of many molecules. This τ_L prediction forms an important benchmark for comparison of experimental results and more realistic theoretical models.

Solvation times are measured experimentally by following the time-dependent shift of the fluorescence spectrum of a dipolar probe solute after ultrafast excitation. Recently, several groups have made such measurements on a wide range of solute/solvent combinations.[15–20] A number of general observations can be made based on the results to date. Solvation times are often close to, but nearly always longer than τ_L. In solvents with very high dielectric constants, observed times can be more than an order of magnitude[16] greater than the τ_L prediction. An approximately linear correlation appears to exist between the ratio of observed solvation time to τ_L and solvent dielectric constant.[21] Finally, the solvation energy typically decays nonexponentially in time.[16] The experimental data thus deviate in several ways from predictions of a homogeneous continuum models. These deviations can most reasonably be assigned to the in-

 0021-9606/88/205044-26$02.10

fluence of molecular aspects of solvation, not accounted for in the simple continuum picture.

A number of more sophisticated theories have recently been proposed that attempt to go beyond a simple continuum description. Inhomogeneous continuum models[22] as well as treatments that explicitly consider the molecular nature of the solvent[23–28] have been reported. In general, these models all predict deviations from simple continuum behavior qualitatively like those observed in experiment. The most applicable of the molecular models, the dynamical MSA model,[26–28] is even able to semiquantitatively reproduce many experimental observations.[21] The insight provided by these studies into the causes for failure of the simple continuum description can be loosely paraphrased as follows: Near to the solute there are insufficient numbers of molecules to attain the full cooperativity required of the τ_L response. Here the response is slower, more single-particle-like than τ_L. Solvent far away, however, does look to the solute like a continuum fluid, and there τ_L pertains. In fact, there is actually a continuous distribution of solvent relaxation times as a function of distance from the solute that ranges between slow, single particle times up to τ_L. Since the net relaxation is a superposition of all of these responses, it is both nonexponential and slower than τ_L. The correlation between the deviation of the actual solvation time from τ_L and the solvent dielectric constant can also be rationalized on this basis.[21,22]

Although substantial experimental and theoretical progress has been made in the last few years, our understanding of the dynamics of solvation is far from complete. More experimental data, especially in high dielectric constant solvents, is needed to verify the generality in the trends discussed above. On the theoretical side, molecular theories have yet to advance to the stage where quantitative agreement with observed behavior has been achieved. More importantly, there are a number of simplifying assumptions common to current theories that need to be explored before we can be confident that even the correct qualitative picture has been reached. Two of the most important are that the solvent behaves linearly with respect to changes in the solute, and that only solvent reorientational mechanisms, i.e., those detected in $\epsilon(\omega)$, are important in the solvation response.

The research reported here is an attempt to provide new data with which to test some of these assumptions. Our "experiments" are molecular dynamics (MD) computer simulations. The molecular level detail afforded by this type of study is vastly superior to that obtained from laboratory experiments and is well suited to investigating the soundness of current models. In this initial study we have focused on simulations of idealized probe solutes in a fairly realistic model solvent. The solutes studied are spherical ions of varying size and charge—the same type of solute considered by theory, but rather far from the complex probe molecules used experimentally. The solvent used is the ST2 model of water.[29] This model provides an accurate representation of many of the properties of liquid water[29,30] and is much closer to an experimental solvent than are the sorts of models employed in theoretical studies.

The choice of water as a solvent was made primarily on the basis of the vast amount already known about aqueous solvation.[31] Especially in terms of computer simulations, the number of studies of aqueous solvation is at least an order of magnitude greater than for all other solvents combined. Traditionally, simulations have mainly concerned the equilibrium structures and energetics of solvation in water. Solutes ranging from simple atomic[32] and ionic[33] species, to complex polyatomic molecules,[34,35] and even the quantum mechanical electron solvation[36,37] in water have been studied in this context. A number of simulations have also addressed dynamical aspects of aqueous solvation. For example, how reorientation and diffusion times of water molecules are perturbed by solutes,[35,38–40] the mechanism of diffusion of simple ions,[41–43] and the dynamical effect of water on an S_N2 reaction[4] have all been studied. While such studies relate to the quantity of interest here, namely the rate at which the solvation energy relaxes after a change in the solute charge distribution, none provides this sort of information directly. Only one study, that of Engström *et al.*[44] concerning quadrupolar relaxation of ions, actually provides solvation rates that can be directly compared with our results. Two further studies have, however, observed other aspects of the response to nonequilibrium changes in an aqueous solute and are closely related to our work. In an early simulation Rao and Berne[45] studied the time scale for structural relaxation after the ionization process $Ne \rightarrow Ne^{2+}$. Very recently, Karim *et al.*[46] have studied the polarization response to changes of the dipole moment of a large spherical solute. Results of these latter studies will also be discussed later.

The format of the remainder of the paper is as follows: Methods used in performing both equilibrium and nonequilibrium MD simulations are described in Sec. II. This section begins by discussing the linear response connection between the time dependence of the solvation process and time correlation functions (TCFs) of appropriate quantities observed in an equilibrium simulation. Details of the solutes studied and simulation algorithms are also provided here. For reasons discussed in Sec. II, we have chosen to carry out simulations in large spherical clusters of water rather than using the more typical periodic boundary conditions. Section III summarizes some of the properties of these clusters. We demonstrate that the environment seen by a solute at the center of such a cluster is virtually indistinguishable from that of bulk ST2 solvent at the experimental density. In Sec. IV we begin the discussion of solvation by examining static aspects of the hydration structures and solvation energies observed for various solutes studied. Although such equilibrium results are not new, they form an important background for understanding the differences in dynamics exhibited by the different solutes. Section V concerns dynamics observed in the equilibrium simulations. How the solutes influence the dynamics of surrounding waters as well as the TCFs related to solvation are presented. In Sec. VI we compare the time-dependent solvation responses obtained in Sec. V to the predictions of the simple continuum model and the dynamical MSA model mentioned above. Neither of these theories provide a quantitative account of the observed behavior and the reasons for this failure are discussed in terms of molecular mechanisms of relaxation. Section VII details the results of

nonequilibrium simulations in which the charge on a solute was jumped and subsequent relaxation observed. Comparison between the observed nonequilibrium response and the response derived from the equilibrium simulations under the linear response assumptions allows us to determine the limits of validity of the linear response approximation. Section VIII concludes with a summary of our main results and a discussion of how these results relate to current ideas about solvation dynamics. Finally, in the Appendix we describe our preliminary determination of the dielectric properties of ST2 water.

II. METHODS

The simulations we have used for studying the dynamics of solvation are of two types. The first is a standard equilibrium MD simulation in which the solute properties are independent of time. From such simulations we obtain information concerning the equilibrium structure and dynamics that exist about specific solutes. Equilibrium simulations also allow for calculation of the solvation response that would result from small variations of the solute's charge distribution. The fluctuation–dissipation theorem connects fluctuations of the electrical potential produced by solvent motions to the dynamic response of the solvent to changes in the solute's electrical properties. We will consider only the linear response regime and thus the equilibrium simulations provide accurate predictions of the solvation response to "small" solute changes. What is meant by a small change can be addressed empirically through comparison with the second type of simulation. In these nonequilibrium simulations we take a preequilibrated sample and at some moment instantaneously alter the solute's charge. We then observe the subsequent evolution of the system and obtain the solvation response directly in time. A summary of all of the simulations is contained in Table I.

Before describing the details of the simulations we first discuss the formalism used to relate nonequilibrium solvation dynamics to the time correlation functions obtained from equilibrium MD. We begin with the general problem of a Hamiltonian which can be broken up into an unperturbed part $H^{(0)}$ and a perturbation H' as

$$H = H^{(0)} + H',$$

where

$$H' = \sum_j X_j F_j(t). \tag{2.1}$$

The perturbation terms $X_j F_j(t)$ couple the system variables X_j to the time-dependent perturbation $F(t)$. In our application, the $F_j(t)$ represent the time varying solute charge distribution and the X_j are components of the electric field produced by the solvent that act on the solute. The first order change in the system due to the perturbation is given by the well-known result[47]:

$$\langle X_i(t)\rangle^{(1)} = \sum_j \int_{-\infty}^{t} F_j(t')\Phi_{ij}(t-t')dt' \tag{2.2}$$

with

$$\Phi_{ij}(t) = \frac{1}{kT}\langle X_i \dot{X}_j(t)\rangle^{(0)}. \tag{2.3}$$

TABLE I. Summary of simulations.

Sim No.	Solute	No. mols	Temp.(K)	Notes
		Equilibrium simulations[a]		
1	···	512	299	
2	···	512	291	250 ps, $dt = 5$ fs
3	$L0$	496	300	
4	$L0$	236	302	
5	$L+$	496	300	
6	$L+$	495	299	
7	$L+$	240	297	
8	$L-$	236	296	
9	$S0$	507	294	
10	$S0$	252	295	
11	$S0$	252	297	
12	$S0$	123	292	
13	$S0$	59	298	
14	$S+\frac{1}{2}$	251	292	
15	$S+$	252	299	
16	$S+$	252	299	$dt = 1$ fs
		Nonequilibrium simulations[b]		
17	$L0 \rightarrow L+$	240	···	$n = 37$
18	$L+\frac{1}{2} \rightarrow L+$	240	···	$n = 36$
19	$L+ \rightarrow L0$	240	···	$n = 40$
20	$L0 \rightarrow L-$	240	···	$n = 40$
21	$S0 \rightarrow S+\frac{1}{2}$	252	···	$n = 40$
22	$S0 \rightarrow S+$	252	···	$n = 40$
23	$S+ \rightarrow S0$	252	···	$n = 27$

Solute designations

Symbol	Description	σ^c	ϵ^c	q(a.u.)
$L0$:	large neutral	2.25	70.0	0.00
$L+$:	large cation	2.25	70.0	+1.00
$L-$:	large anion	2.25	70.0	−1.00
$L+\frac{1}{2}$:	large partial cation	2.25	70.0	+0.50
$S0$:	small neutral	1.00	1.00	0.00
$S+$:	small cation	1.00	1.00	+1.00
$S+\frac{1}{2}$:	small partial cation	1.00	1.00	+0.4444

[a] All equilibrium simulations were of 50 ps duration using a time step of 2 fs unless otherwise noted.

[b] Simulations numbers 17–23 are nonequilibrium simulations in which the charge was jumped in the direction described by $L0 \rightarrow L+$, etc. n here designates the number of jumps performed.

[c] Solute–solute LJ parameters σ and ϵ are given in units of the LJ parameters of the ST2 water model ($\sigma = 3.10$ Å, $\epsilon = 0.075\,75$ kcal/mol). The solute–solvent LJ interactions were calculated from these using the usual Lorentz–Berthelot combining rules.

The pulse response function $\Phi_{ij}(t)$ describes the linear response of the ensemble-averaged (denoted by $\langle\ \rangle$) system property X_i to a delta function F_j perturbation. (The superscript 1 on $\langle X_i(t)\rangle$ denotes that this is the change to first order in F.) Equation (2.3) relates this pulse response function to a time correlation function of the system variables in the absence of the perturbation. In this expression $\dot{X}$ represents the time derivative of X and the $\langle\ \rangle^{(0)}$ denotes an ensemble average calculated with $H = H^{(0)}$. We will be concerned with the response to a step function change in solute properties, so we consider $F(t)$ of the form

$$F_j(t) = \begin{cases} 0, & t<0 \\ F_j, & t \geqslant 0 \end{cases}. \tag{2.4}$$

For such an $F(t)$, Eq. (2.2) can be integrated to yield

$$\langle X_i(t)\rangle^{(1)} - \langle X_i(\infty)\rangle^{(1)} = \frac{1}{kT}\sum_j F_j\,[\langle X_i X_j(t)\rangle^{(0)} - \langle X_i\rangle^{(0)}\langle X_j\rangle^{(0)}], \tag{2.5}$$

where $\langle X_i(\infty)\rangle$ denotes the value of X_i when the system has equilibrated to the perturbation. Equation (2.5) is the general fluctuation–dissipation expression we will use to obtain the solvation response from our equilibrium simulations.

We now specialize the above general result so as to consider the solvation response to changes in the first three multipole moments of a solute's charge distribution. In particular, we will examine the relaxation of the solvation energy after step function changes in either a point charge, dipole, or axial quadrupole located at the center of the solute. The electrostatic free energy of solvation of such point multipoles can be written

$$E_{\rm solv}(t) = \begin{cases} 1/2q(t)\langle V(t)\rangle & \text{charge} \\ -1/2\mu_z(t)\langle E_z(t)\rangle & \text{dipole} \\ -1/2Q_{zz}(t)\langle V_{zz}(t)\rangle & \text{quadrupole} \end{cases}, \tag{2.6}$$

where q is the magnitude of the charge and μ_z and Q_{zz} are the magnitudes of the dipole and quadrupole moments which are assumed to lie along the z direction. The quantities V, E_z, and V_{zz} are the appropriate electric potential, field, and field gradient ($-\partial^2 V/\partial z^2$) components at the site of the multipole induced by its interaction with the solvent. Similar expressions, without the factors of 1/2 and the ensemble averaging, also provide the perturbation terms in the Hamiltonian, Eq. (2.5), with changes in q, μ, and Q being the F terms and the reaction fields V, E_z, and V_{zz} being the system properties X. For simplicity we will consider only the effect of changes in magnitude of the dipole and quadrupole rather than allowing the direction to change as well. (Under this restriction the i–j cross correlations that would otherwise arise between different field components do not contribute.)

Let us consider the quadrupole case as an example. The time-dependent perturbation corresponding to a step function change in quadrupole moment of magnitude ΔQ_{zz} is

$$H' = V_{zz}\Delta Q_{zz} \tag{2.7}$$

and the response to the solvation free energy $\Delta E_{\rm solv}(t)$ to such a change is given to first order by

$$\begin{aligned}\Delta E^{(1)}_{\rm solv}(t) - \Delta E^{(1)}_{\rm solv}(\infty) &= -\frac{1}{2}Q_{zz}[\langle V_{zz}(t)\rangle^{(1)} - \langle V_{zz}(\infty)\rangle^{(1)}] \\ &= -\frac{1}{2kT}Q_{zz}\Delta Q_{zz}[\langle V_{zz}V_{zz}(t)\rangle^{(0)} - \langle V_{zz}\rangle^{(0)}\langle V_{zz}\rangle^{(0)}] \\ &= -\frac{1}{2kT}Q_{zz}\Delta Q_{zz}\langle \delta V_{zz}\delta V_{zz}(t)\rangle. \end{aligned} \tag{2.8}$$

In these expressions Q_{zz} denotes the total magnitude of the quadrupole moment after the ΔQ_{zz} change and δV_{zz} is the fluctuation in the zz field gradient component. The superscripts (1) and (0) again designate that the energies are correct to first order in H' and that the ensemble averaging of the V_{zz} quantities is performed in the absence of H'. We will hereafter omit these superscripts.

Equations analogous to Eq. (2.8) for the charge and dipole cases are obtained by substituting the appropriate quantities for V_{zz} and Q_{zz}. For discussing the solvation time dependence it is usually more convenient to work with the normalized response function $S(t)$ defined by

$$S(t) = \frac{\Delta E_{\rm solv}(t) - \Delta E_{\rm solv}(\infty)}{\Delta E_{\rm solv}(0) - \Delta E_{\rm solv}(\infty)} \tag{2.9}$$

rather than with the energies themselves. Within the linear response approximation, the $S(t)$ response functions appropriate to step changes in the three point multipoles are equal to three normalized time correlation functions $[C(t)]$ as follows:

Equilibrium TCF		Nonequilibrium response
$\dfrac{\langle \delta V \delta V(t)\rangle}{\langle \delta V^2\rangle}$		Δq
$\dfrac{\langle \delta E_z \delta E_z(t)\rangle}{\langle \delta E_z^2\rangle}$	$C(t) \leftrightarrow S(t)$	$\Delta\mu_z$
$\dfrac{\langle \delta V_{zz}\delta V_{zz}(t)\rangle}{\langle \delta V_{zz}^2\rangle}$		ΔQ_{zz}

(2.10)

These equations represent the desired final result connecting the temporal decay of fluctuations in the quantities V, E_Z, and V_{zz} that we collect from the equilibrium MD simulations to the nonequilibrium solvation response $S(t)$.

All of the simulations reported here involve spherical solutes fixed at the center of spherical clusters of water solvent. The use of clusters for these studies has two advantages over the more usual periodic boundary conditions. First, maintaining spherical symmetry is helpful in that it allows for the maximum possible averaging of observables since all properties have only radial dependence. Thus, e.g., V_{zz} in Eq. (2.9) is equivalent to V_{xx} and V_{yy}, so that the correlation functions we report for $\langle \delta V_{zz}\delta V_{zz}(t)\rangle$ are actually averaged over the independent x, y, and z directions. Second, by avoiding periodic boundary conditions we avoid having to make approximate corrections for the long-ranged interactions across cell boundaries. It has only been after many years of debate that the use of reaction field[48] or Ewald summation[49] techniques for treating periodic boundary conditions in polar solvents now seems to be well understood.[50] With clusters we bypass the complications involved with these techniques and work with a simple, well defined model system whose simulation involves no such approximations. The main drawback of using clusters is of course that the simulated system incorporates a large fraction of molecules near to the surface of the cluster that have properties different from those in the bulk. In order to study solvation in the liquid phase we must work with clusters sufficiently large that edge effects do not significantly affect the results.[51] As we will discuss in Sec. III we have found clusters containing 256–512 solvent molecules to be adequate for the solvation properties of interest here.

The water–water potential chosen in this work is the ST2 model of Stillinger and Rahman.[29] A water molecule in this model consists of a single Lennard-Jones center at the oxygen position ($\sigma = 3.1$ Å and $\epsilon = 0.076$ kcal/mol) and four partial charges of magnitude 0.24 e tetrahedrally arranged about this site that represent the two hydrogens and two oxygen lone pairs. The hydrogen positions are 1 Å from the oxygen whereas the negative charges are at a distance of 0.8 Å, producing a slight charge asymmetry in the molecule. Solutes are constrained to the center of the cluster and interacted with the water solvent via a (6-12) Lennard-Jones term plus Coulomb terms between the water charges and a centered point charge. Details of the solute parameters are provided in Table I. No interaction cutoffs were employed in this work so that all water–water and water–solute interactions were explicitly included in the calculations. The cluster was maintained using a spherical confining potential that reflected waters attempting to evaporate from the cluster. Even at 298 K water molecules are sufficiently strongly bound that few molecules attempt to leave the cluster during a 50 ps simulation. The placement of the confining potential was chosen such that its presence had no observable effect on the cluster properties.

Integration of the equations of motion was performed using the Verlet algorithm[52] and the rigid body constraints of the ST2 waters were maintained with the SHAKE[53] and RATTLE[54] methods. A time step of 2 fs was used in almost all simulations (Table I lists the exceptions). This step size provided energy conservation to better than 2% over the course of 50 ps for pure ST2 clusters. Energy conservation for the small charged solutes was somewhat poorer (due to the lack of a switching function in the solvent–solute interactions) so that the kinetic energy had to be rescaled several times during the course of some of these runs. Comparison of runs No. 15 and No. 16 showed that the influence of time step had little influence on the observed solvation dynamics.

The equilibrium MD simulations typically consisted of a 5–10 ps equilibrium period followed by a 50 ps production run during which data were collected. Rather than saving all solvent coordinates, which would require excessive storage for the large samples used, most observables were calculated during the course of the run. Exceptions were the electrical properties used in evaluating the solvation dynamics, which were continuously output. The nonequilibrium simulations were performed by running two calculations in parallel. The first was a simulation in equilibrium with respect to the initial state of the solute; this was used to obtain starting points for the nonequilibrium simulations. The second, nonequilibrium series of simulations were run using initial conditions chosen from the equilibrium run at 1 ps intervals. In the nonequilibrium runs the charge of the solute was instantaneously changed and the dynamics in the presence of the altered solute then followed for 1 ps. Typically, a series of 40 charge jumps were simulated to produce averaged results. In both the equilibrium and nonequilibrium simulations, properties were examined as a function of distance from the solute by dividing the system up into a series of 3–5 shell regions. The first and last shells were defined so as to respectively include only waters that were nearest neighbors of the solute and surface waters, respectively (as judged by the solute/solvent radial distribution function). The other shells evenly divided the remaining radial space.

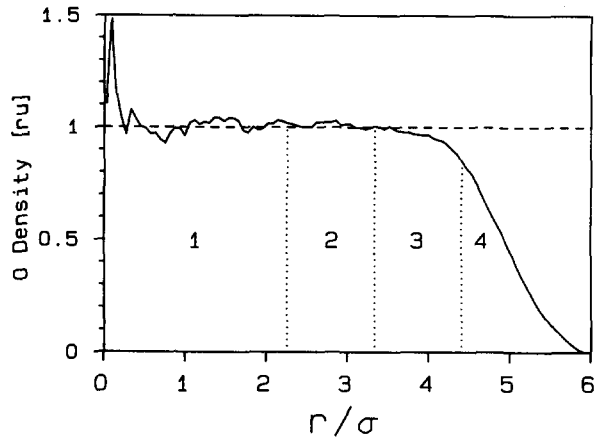

FIG. 1. Water oxygen radial density profile of a pure 512 molecule cluster. Units are relative to the ST2 LJ diameter σ. The numbers 1–4 mark the shell regions used in collecting data.

III. PURE SOLVENT CLUSTERS

Before describing the solvation results we first discuss the nature of the solvent environment provided by the water clusters used in these studies. Our main emphasis will be to show that clusters containing 256 or 512 solvent molecules are in most respects indistinguishable from the neat liquid. We also describe a few features unique to the surfaces of these clusters.

Figure 1 shows the radial density profile of a cluster of 512 ST2 molecules at 298 K. Distances in this and remaining figures are given in units of the LJ diameter of the ST2 model, $\sigma = 3.10$ Å. We have examined how properties vary as a function of radial position by dividing the sample into the four regions marked in the figure. With few exceptions the properties of water molecules in shells 1–3 are identical but differ significantly from waters in the outermost region 4. The dashed line in Fig. 1 denotes the experimental density of water at this temperature. As far as the density is concerned, the region out to about 4σ is bulk-like for a cluster of this size. The density falloff in the surface region takes place in approximately one molecular diameter and is well represented by a function of the form $\rho(r) = 0.5\rho_0\{1 - \tanh[2(r - r_0)/\lambda]\}$ with $\lambda = 1.1\sigma$.[55]

In Table II a number of static and dynamic properties calculated from a simulation of a 512 molecule cluster are compared to results obtained by others for the ST2 model in periodic boundary simulations, and to experimental data for water at 298 K. The density of the interior of the cluster is $\sim 1\%$ low of the experimental value, which is considerably closer agreement than is achieved in periodic simulations at 1 atm. As pointed out by Townsend *et al.*[55] this fortuitous improvement seen in cluster simulations is due to the pressure exerted by the curved surface of the cluster. The poten-

TABLE II. Pure cluster properties (298 K).

Property	Cluster $N=512$[a] Surface	Interior	Periodic[b] simulation	Experiment
Density ($g\,cm^{-3}$)	···	0.988	0.925[c]	0.997[c]
$-V/N$(kcal/mol)[d]	~7.2	~10.2	10.4[e]	9.9[c]
τ_{1d}[e] τ_{exp}	6.9	7.8	~5[f]	~6[g]
$\langle\tau\rangle$	6.0	7.2	8.2 (281 K)[i]	···
τ_{2H}[e] τ_{exp}	2.2	2.6	2.4[j]	···
$\langle\tau\rangle$	1.1	1.8	1.7[j]	2.5[k]

[a] "Surface" waters were taken to be all molecules lying outside of a radius of $r=4.4\sigma$. At this radius, the density has decreased to ~90% of the bulk density. All other waters were considered to be "interior" waters.
[b] The density value listed here is from a 1 atm constant-pressure simulation (c). The remaining values are from constant volume simulations in which the density was constrained to be unity.
[c] Values from W. Jorgensen, J. Chandrasekhar, J. D. Madura, R. W. Impey, and M. L. Klein, J. Chem. Phys. **79**, 926 (1983).
[d] V/N is the potential energy per molecule. For the clusters, division into surface and interior components was done approximately, as described in the text.
[e] From R. A. Kuharski and P. J. Rossky, J. Chem. Phys. **82**, 5164 (1985).
[f] Time constants of the $l=1$ dipole and $l=2$ H–H vector reorientational TCFs described in the text [Eqs. (3.1) and (3.2)].
[g] Approximate value based on data from short simulations reported in A. Geiger, Ber. Bunsenges. Phys. Chem. **85**, 52 (1981); A. Geiger, A. Rahman, and F. H. Stillinger, J. Chem. Phys. **70**, 263 (1979).
[h] Approximate value based on a dielectric relaxation time of $\tau_D=8.3$ ps and using the approximate relation $\tau_{d1}\sim\{3\epsilon_0/(2\epsilon_0+\epsilon_\infty)\}\tau_D$ (see the text).
[i] D. A. Zichi and P. J. Rossky, J. Chem. Phys. **84**, 2814 (1986).
[j] Gy. I. Szasz and K. Heinzinger, J. Chem. Phys. **49**, 3467 (1983).
[k] NMR result of J. Jonas, T. DeFries, and D. J. Wilbur, J. Chem. Phys. **65**, 582 (1976).

tial energy per water in the interior of the cluster we estimate to be essentially identical to that observed in other simulations and to estimates of the experimental value. We did not actually calculate the total potential energy per molecule in each region but rather only the local bonding energy arising from interactions between molecules separated by less than 1.5σ. The bonding energies so calculated were the same for shells 1–3. For surface waters the distribution of local bonding energies was shifted to more positive energies by about 3 kcal/mol, which is ~2/3 of the energy of a typical hydrogen bond in the ST2 model (4.5 kcal/mol). The estimates of the total potential energies listed in Table II were calculated from the total cluster potential energy by assuming that this difference in local bonding energies accounted for all of the energetic difference between the two classes of molecules.

The dynamics of water molecules in the interior of the cluster was also independent of position throughout regions 1–3 but considerably faster in region 4. In Fig. 2 we illustrate the difference in dynamics using two reorientational time correlation functions (TCFs). These correlation functions are defined by

$$C_{l_i}(t)=\langle P_l[\hat{u}_i\cdot\hat{u}_i(t)]\rangle, \tag{3.1}$$

where P_l denotes a Legendre polynomial of order l and u_i is a unit vector in the molecular frame. Here we have plotted the correlation functions $C_{1d}(t)$ and $C_{2H}(t)$ which involve the unit vectors in the dipole (d) and H–H bond (H) directions. These functions are not strictly exponential at long times due to the exchange between interior and surface waters. (For calculating these TCFs we assign molecules to regions only once every 5 ps.) In Table II we compare characteristic time constants of these TCFs to experimental and simulated values. The two time constants listed are τ_{ex}, which is based on an exponential fit of $C(t)$ between 1–5 ps, a region that excludes the fast librational component of the motion, and the average time $\langle\tau\rangle$,

$$\langle\tau\rangle=\int_0^\infty C(t)dt \tag{3.2}$$

which does include this fast component. The reorientation times we observe in the interior of the clusters are in good agreement with times measured by others in bulk ST2 simulations. We note that our values for these quantities are more

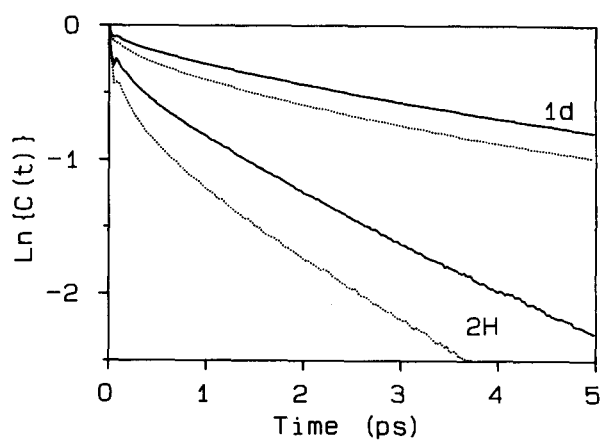

FIG. 2. Reorientational time correlation functions of the water dipole (1d) and H–H (2H) vectors in a pure (512) cluster. The first ($l=1$; 1d) and second ($l=2$; 2H) order Legendre TCFs [Eq. (3.1)] are plotted for two different regions in the cluster. Solid lines are for molecules in the bulk regions 1–3 and dotted lines correspond to surface waters (region 4) as defined in Fig. 1.

reliable than most available in the literature since the latter are typically based on simulations of only a few picoseconds duration. The times for bulk ST2 water are also in reasonable accord with the dynamics of real water. The value of $\langle \tau_{2H} \rangle$ is obtained from NMR measurements and is directly comparable to the simulated quantity. The experimental value of $\tau_{1d} \sim 6$ ps is only a rough estimate obtained using the relation due to Powles[56] between this single particle time and the dielectric relaxation time of $\tau_D = 8.3$ ps.[57] The ST2 model results are within 30% of the experimental values for both of these dynamical properties. Reorientation of surface waters is faster than that of bulk water by a factor of 5%–40% depending on which measure is used. It may seem somewhat surprising that the surface waters are not much faster than bulk waters, however, the small difference actually observed is in keeping with the fact that roughly three hydrogen bonds are still maintained at the surface.

One final aspect of the pure solvent clusters of interest is the orientation of waters at the surface. Several studies have previously shown that water[55,58,59] and other polar molecules[60] tend to orient such that their dipole direction lies parallel to the cluster surface. This phenomenon is illustrated in Fig. 3(A) for a 512 molecule cluster. Here we show the cosine distribution of the angle made between the dipole direction and the radius vector as a function of radial shell. There is a strong preference for dipolar orientation perpendicular to the radial direction for molecules in the surface layer (shell No. 4, solid curve). This preference also propagates to the interior layers, although the orientation is small for regions 1 and 2. These orientational correlations are one of the few properties for which there is a difference observed among interior shell regions Nos. 1–3. In addition to dipolar orientation there is a preferential orientation of the H–H direction relative to the radius vector as shown in Fig. 3(B). In this case the distinction between different internal layers is negligible and only the surface layer shows much of an effect. The preferred arrangement of exterior waters is for the dipole to point parallel to the cluster surface and for the HOH plane to be perpendicular to this surface. Compared to the bulk, a surface molecule with such an orientation has chosen to give up one H atom for hydrogen bonding by projecting it out from the cluster rather than doing the same with one of its negative charge sites (Q). The distinction between H and Q is due to the small asymmetry in the O–H and O–Q bond lengths in the ST2 model, 1.0 compared to 0.8 Å, respectively. We note that such preferential orientation leads to a net positive surface charge in ST2 clusters as was recently observed by Brodskaya and Rusanov[59] in much smaller clusters.

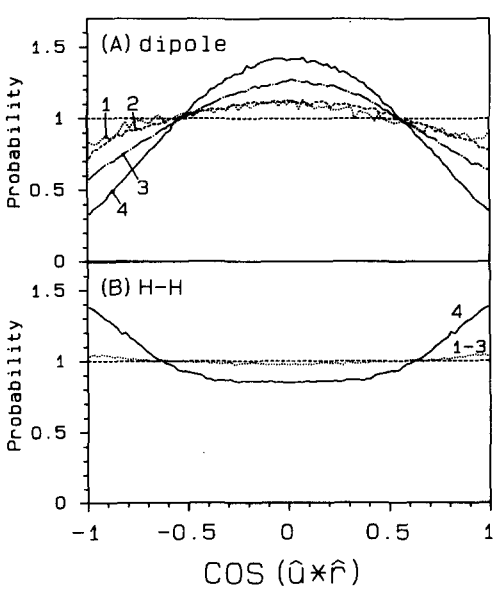

FIG. 3. Angular distributions of water molecules in a 512 cluster as a function of position. The angular variable is $\cos(\hat{u}^*\hat{r})$ where r is the vector from the cluster center to the oxygen position and u is a molecule fixed vector specifying (A) the dipole direction, and (B) the H–H internuclear direction. (We define the dipole direction to point from O to the H–H bisector.) Probabilities have been scaled such that a random distribution would correspond to $P = 1$. In panel (A) distributions for all four regions of the cluster (Fig. 1) are shown. The distributions of the H–H vector were virtually identical in regions 1–3 and in panel (B) we show only the average distribution.

We have centered the preceding discussion around pure clusters of size $N = 512$. Essentially the same features are also observed for the clusters of 256 molecules which we also employ in our solvation studies. In clusters of both sizes there is a surface region of thickness $\sim 1\sigma$ in which molecules are less strongly bound, have a preferential orientation, and reorient slightly faster than in bulk water. The remainder of the cluster is indistinguishable from bulk water with the exception of there being a slight residual preference for molecules to align with their dipoles perpendicular to the radial direction. This residual orientation does not noticeably affect the observed energetics or dynamics of interior waters and should not influence our solvation results significantly. The primary difference between clusters of size 512 vs 256 is simply the numbers of molecules contained in the surface and interior regions. For clusters of size 512 the numbers are approximately $N_{surf} \sim 162$ (32%) and $N_{int} \sim 350$ (68%) and for 256 clusters they are $N_{surf} \sim 106$ (41%) and $N_{int} \sim 150$ (59%). How the presence of surface water influences the solvation properties depends of course on the range of the relevant interactions considered and will be discussed later.

IV. SOLVATION STRUCTURE AND ENERGETICS

We have performed equilibrium simulations with six solutes that we designate $L0, L+, L-, S0, S+\frac{1}{2}$, and $S+$ (see Table I). These solutes are of two sizes "L = large" and "S = small." The small solutes have Lennard-Jones parameters identical to those of the ST2 oxygen center: $\sigma_{SS} = 3.1$ Å, and $\epsilon_{SS} = 0.076$ kcal/mol. The 0, $+\frac{1}{2}$, and $+$ descriptors on the small solutes designate 0, $+0.4444$, and $+1$ units of atomic charge at the solute center. Large solutes all have LJ parameters $\sigma_{LL} = 70$ and $\epsilon_{LL} = 5.3$ kcal/mol. The 0, $+$, and $-$ again denote 0, $+1$, and -1 charge. The rationale behind the choice of LJ parameters for the large solutes was to simulate a system of roughly the volume and polarizability of the probe molecules employed in fluorescence Stokes shift measurements. The small solutes were used to examine size effects on solvation dynamics and are intended more to represent small polar groups in a large molecule rather than to closely resemble common ions. In all simulations the solutes were immobilized at the center of the

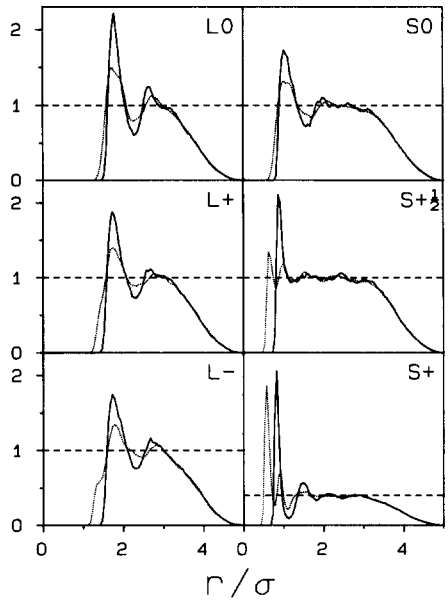

FIG. 4. Summary of solute–water radial distribution functions for all solutes studied (256 clusters). The solid curves are the Sol–O distribution and the dotted curves are either the Sol-Q ($L0, L+, S0, S+, S+\frac{1}{2}$) or Sol–H distributions ($L-$) where O, Q, and H denote the water oxygen, negative charge, and hydrogen sites, respectively.

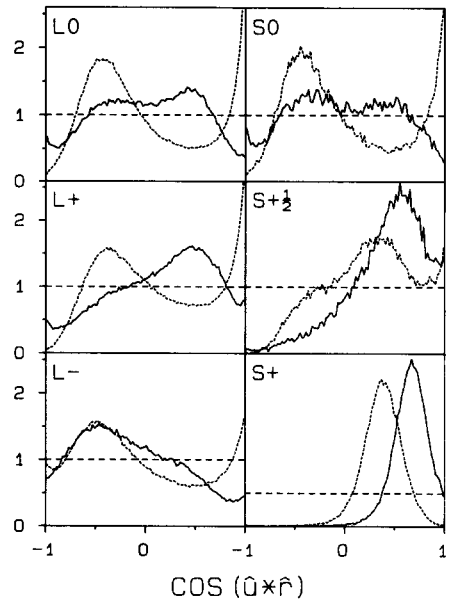

FIG. 5. Summary of the angular distributions of water molecules in the first solvation shells of the 6 solutes studied (256 clusters). The angular variable is $\cos(\hat{u}*\hat{r})$ where r is the vector from the solute center to the water oxygen position and u is a water-fixed vector. Solid lines are for u = the dipole direction and dashed lines are for u = the O–H bond direction (pointing from O to H). Probabilities have been scaled such that a random distribution would correspond to $P = 1$.

solvent cluster. This constraint is consistent with the approach of most theoretical studies of solvation dynamics and, based on previous simulations of ion motion,[43] should have negligible effect on the dynamics of interest.

Figures 4 and 5 and Table III document some features of the solvation structure that exists about these solutes. These data are from simulations of 256 molecule clusters (see Table III), however, results are unchanged in larger clusters. Figure 4 shows the radial distribution functions (RDFs) of the distances between the solute ("Sol") and two interaction sites of the ST2 solvent. In all but the L case, the water sites displayed are the oxygen atom (O) and negative charge (Q) positions. For the L solute the water hydrogen atoms (H) are shown instead of the negative charge sites. The Sol–O RDFs are similar for all of the large solutes and for $S0$. There is a fairly broad but clearly defined first shell region and, in addition, a small maximum denoting a second neighbor shell. The small charged solutes have a much sharper first neighbor peak (note vertical scale difference for $S+$) in their Sol–O RDF which is also closer to the solute by 0.1–0.2σ. Solvation numbers, determined from areas under the first peak, range from 7 for $S+\frac{1}{2}$ and $S+$, to 16 for $S0$, to $\sim$40 for all of the large solutes (Table III). The distribution

TABLE III. First shell solvent properties.

	O–solute radial distribution[b]						Water–water energetics[c]		
Solute	No. nn[a]	$r(1+)$	$\rho(1+)$	$r(1-)$	$\rho(1-)$	$r(2+)$	E_{bind}	ΔE_{bind}	No. N_{hb}
$L0$	42	1.80	2.20	2.28	0.6	2.6	16.5	9	3.7
$L+$	40	1.75	1.87	2.28	0.7	2.26	15.5	10	3.5
$L-$	43	1.75	1.73	2.33	0.7	2.6	15.5	10	3.5
$S0$	16	1.05	1.72	2.61	0.7	1.9	16.5	9	3.7
$S+\frac{1}{2}$	7	0.90	2.10	1.2	1.0	···	12.5	11	2.8
$S+$	7	0.83	5.16	1.12	0.22	1.5	3.0	11	0.7
						(bulk:	16.0	10	3.6)

[a] Number of water molecules in the first solvation shell as measured by the integral under the solute–oxygen RDF up to the first minimum [$r(1-)$].

[b] Characteristics of the solute–oxygen radial distribution functions. r designates a distance from the solute in units of the ST2σ(3.10 Å) and ρ is the solvent oxygen density in units of molecules/σ^3 [the average density is essentially unity so that these values are equivalent to values of $g(r)$]. The designations $1+$, $1-$, and $2+$ refer, respectively, to the first maximum and minimum and second maximum of the RDFs.

[c] The binding energy (kcal/mol) of a molecule is defined here as the potential energy of interaction of the molecule with all neighboring water molecules within a distance of 1.5σ. The values E_{bind} and ΔE_{bind} refer to the energy at the maximum and FWHM of the distribution of binding energies of first shell waters. N_{hb} is the number of hydrogen bonds calculated from E_{bind} using an average H-bond energy of 4.5 kcal/mol from pure water simulations.

TABLE IV. Solute–solvent energies.

Solute	N_{solv}	Sim No.[a]	E_{sw} (Tot)[b]	E_{sw} (vdW)[b]	E_{sw} (El)[b]	%E(Shell 1)[c]
$L0$	496	3	−32.9	−32.9	···	···
$L0$	236	4	−30.9	−30.9	···	···
$L+$	496	5&6	−96.2	−29.9	−66.3	57
$L+$	240	7	−88.7	−28.5	−60.2	62
$L-$	236	8	−89.7	−28.0	−61.7	57
$S0$	507	9	−0.36	−0.36	···	···
$S0$	252	10&11	−0.44	−0.44	···	···
$S0$	123	12	−0.43	−0.43	···	···
$S0$	59	13	−0.21	−0.21	···	···
$S+\frac{1}{2}$	251	14	−32.7	+1.8	−34.5	64
$S+$	252	15&16	−179.0	+13.2	−192.0	66

[a] These data are separated according to solute and cluster size (N_{solv}). In cases where more than one simulation is listed the values shown are averages.

[b] Potential energies of solute–water interactions E_{sw} in kcal/mol. The energy is decomposed into contributions due to van der Waals (vdW) and electrostatic ($E1$) terms in the solvent–water interaction.

[c] %E(shell 1) is the percentage of E_{sw} ($E1$) due to first solvation shell waters.

functions for the charge sites differ in the expected manner between the charged and uncharged species. Thus for $L0$ and $S0$, the Sol–Q and Sol–H RDFs are indistinguishable, whereas for the charged solutes there is an excess of oppositely charged sites close to the solute.

Figure 5 shows the angular distributions of solvent molecules in the first solvation shell. The two angles depicted are those between the Sol–O radius vector and the dipole direction (solid), and the radius vector and the O–H bond direction (dashed curves). The solvation structures that can be deduced from these angular distributions and the radial distribution functions are well known from previous water simulations.[32,33,38] All of the large solutes, as well as $S0$, exhibit characteristics of "hydrophobic" solvation. Waters in the first solvation shell tend to form a clathrate-like structure around the solute, pointing three of their four charge sites tangentially to the solute surface and the fourth radially outward. By so doing virtually the same amount of hydrogen bonding that is present in bulk water can be preserved. (Quantitative comparisons between the water–water binding energy distributions of first shell solvent are provided in Table III). There are some differences between the angular distributions of the L solutes depending on charge but these represent a modest perturbation on the dominant hydrophobic theme. Thus the dipole distributions of $L+$ and $L-$ are skewed so as to bias the charge distribution slightly in the appropriate directions. Based on the areas under the small-r shoulders in the Sol–Q and Sol–H RDFs of $L+$ and $L-$, however, we estimate that fewer than 10% of the solvent molecules actually point a charge directly at the solute. (Note also that the dipole distributions of the uncharged solutes are already slightly asymmetric such that there is a small negative potential near the solute.) Solvation of the $S+$ solute represents the opposite extreme from that of the L solutes, namely hydrophilic hydration. The structure here is one in which first shell waters are very strongly oriented so as to point one of their negative charge sites directly at the solute (Fig. 5, again note the vertical scale difference). First shell waters give up favorable interactions with one another in order to pack as closely to the solute as possible and thereby maximize the solute–solvent attraction. As can be seen from Table III, less than 1/5 of the water–water binding energy of the bulk is preserved in the first solvation shell of $S+$. The final solute, the partially charged $S+\frac{1}{2}$, is a case intermediate between the hydrophobic and hydrophilic extremes. All of the features of its solvation structure appear to reflect a superposition of those of solutes $S0$ and $S+$, in roughly comparable amounts. This superposition is evident in the radial distribution functions, the angular distributions, and in the water–water energy distributions.

The energetics of solvation are considered in Table IV and Fig. 6. We have not attempted to calculate solvation free energies and so we compare only relative solute–water interaction energies, E_{sw}. Several points can be made on the basis of these energies. First, the total E_{sw} is somewhat dependent on the size of the cluster. This is to be expected for ionic solutes. The electrostatic energy of interaction between a charge and the polarization it induces in the solvent a distance r away varies as r^{-3} for large r. Modeling a cluster as a

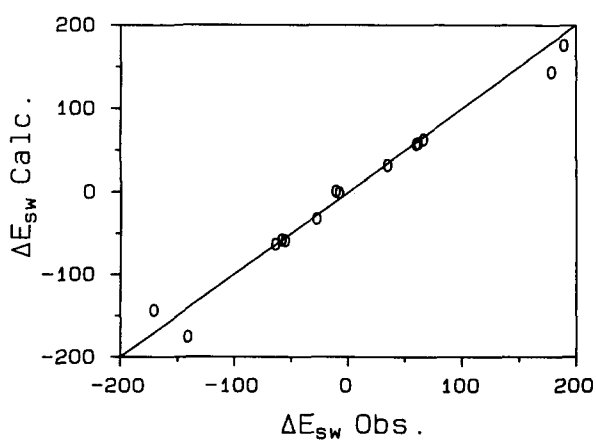

FIG. 6. Observed vs calculated solvation energy differences (ΔE_{sw}, kcal/mol) between solutes with different charges. The observed values were calculated from the E_{sw} data in Table IV and the calculated values were obtained using the linear response result [Eq. (4.1)] (see the text).

TABLE V. Continuum estimates of cluster size effects.[a]

Cluster size	Percentage missing 512	256	128	64
Property		*S* solute		
V	10	13	16	21
E_z	0.1	0.2	0.4	0.9
V_{zz}	0.001	0.003	0.01	0.04
		L solute		
V	23	29	36	47
E_z	1.2	2.4	4.8	10
V_{zz}	0.06	0.2	0.6	2.3

[a] Values listed are the percentage of the total electrostatic solvation energy of an infinite sample that is missing when a finite cluster is used. These numbers are based on treating the solvent as a continuum as discussed in the text. V, E_z, and V_{zz} refer to the energies of solvation of a point charge, dipole, and quadrupole, respectively.

homogeneous dielectric sphere, the fraction of the bulk solvation energy of an ion of radius r_0 in a cluster of radius R is given by $1-(r_0/R)$. The fractions of the bulk electrostatic solvation energy of an L size ion expected for 512 and 256 molecule clusters are thus calculated to be 77% and 71%, respectively. The analogous fractions for S size solutes are 90% and 87%. (See also Table V.) The observed ratio of E_{sw} for $L+$ in the 512 and 256 clusters is close to what is expected on this basis. Table IV also lists the part of E_{sw} due to van der Waals interactions. In the following sections we will be interested in the time dependence of the solvation energy in response to a change in solute charge. Comparing changes in the total E_{sw} to changes in the van der Waals component one sees, as expected, the major effect is in the electrostatic component of E_{sw}. The van der Waals energy also changes as a result of changes in the first shell structure, however, this is a secondary effect and amounts to less than 7% of the total energy change in all cases. In the remaining analysis we therefore concentrate exclusively on the energetics of the electrostatic interactions and ignore the second order changes in the van der Waals energies.

It is also instructive to examine what fraction of the electrostatic part of E_{sw} comes from interactions with the first solvation shell. As shown in Table IV, even for the large solutes, over half of the energy comes from nearest neighbor interactions. The observed fractions are close to what would be expected from a continuum calculation of the sort described here. For example, a region between the van der Waals radius of $L+$ and the first minimum in the $L+$ RDF contributes 71% of the solvation energy of $L+$ immersed in a homogeneous dielectric sphere of size appropriate to a 256 cluster. The observed fraction is 62%. It is interesting that such continuum estimates should yield answers within ~20% of the observed values.

In Sec. V we will calculate the nonequilibrium response to a step change in solute charge assuming the solvation energy varies linearly with the size of the charge jump. By comparing E_{sw} for the different solutes listed in Table IV we might hope to determine what magnitude of charge jump is consistent with this linear response assumption. From the analysis of Sec. II it is possible to calculate the difference in electrostatic energy between solutes that differ only in their charge, based on solvent properties in the presence of either one of the solutes. Denoting the two solutes a and b and their charges q_a and q_b, the relation

$$E_{sw}(a)-E_{sw}(b)=(q_a-q_b)\left\{\langle V\rangle^{(b)}-\frac{q_a}{kT}\langle\delta V^2\rangle^{(b)}\right\} \tag{4.1}$$

should hold if the linear approximation is valid. The quantities $\langle V\rangle^{(b)}$ and $\langle\delta V^2\rangle^{(b)}$ are the average electrical potential and the square of its fluctuation in the presence of solute b. (Values of these quantities are listed in Table VII.) Figure 6 compares the observed E_{sw} differences to those calculated on the basis of Eq. (4.1). There are 14 points on this plot corresponding to 7 pairs of solute/cluster systems that differ only in solute charge. [While there are only seven independent observed ΔE_{sw} values there are twice this number of calculated differences since either system can serve as the reference in Eq. (4.1).] The agreement between the observed and predicted energy differences is fairly good. Such agreement is not surprising when differences between large solutes (ΔE_{sw} between $\pm$ 100 kcal/mol) are considered, since, as we have shown, the solvation structure about these solutes is relatively insensitive to charge. The fact that the observed E_{sw} between $S0$ and $S+$ (extreme points) are also within $\pm$ 20% of the linear predictions is quite surprising however. The solvation structures about these two solvents are very different. Furthermore, the per-molecule contribution of first shell waters to the solvation energy difference is ~18 kcal/mol, which is larger than the water–water binding energy in the bulk. In this sense the perturbation caused by charging $S0$ can hardly be considered small and the agreement with the linear prediction must be partly fortuitous.

A final aspect of the equilibrium solvation properties we will consider is a more direct comparison of the observed energetics to predictions of simple models of solvation. We will later use these same models to compare to our dynamical results. The free energy of solvation of an ion is determined by the reaction potential as described by Eq. (2.6). This reaction potential is simply the electrical potential at the charge site that is due to the ion's polarization of its surroundings. Observed values can be obtained from differ-

TABLE VI. First shell reorientation times.[a]

Solute	$\langle\tau_{2H}\rangle_{1st}$	$\langle\tau_{2H}\rangle_B$	Ratio first bulk
$L0$	2.3	1.6	1.4
$L+$	2.3	1.7	1.4
$L-$	1.8	1.9	1.0
$S0$	3.6	2.1	1.7
$S+\frac{1}{2}$	2.3	1.9	1.2
$S+$	3.2	1.8	1.8

[a] Integral time constants [$\langle\tau_{2H}\rangle$, Eq. (3.2)] of the $l=2$ H–H vector reorientational correlation function [Eq. (3.1)] for the first solvation shell (1st) and bulk (B) water. All data are from simulations of clusters of size 256. Bulk values are averages over all molecules not within the first solvation shell or the surface region.

TABLE VII. Static electrical properties.[a]

Solute	N_{solv}	$\langle V\rangle$ ×10	$\langle V_{zz}\rangle$ ×10^3	$\langle \delta V^2\rangle$ ×10^4	$\langle \delta E_z^2\rangle$ ×10^6	$\langle \delta V_{zz}^2\rangle$ ×10^6	First shell $\langle \delta V^2\rangle$ ×10^4	First shell $\langle \delta E_z^2\rangle$ ×10^6
$L0$	496	−0.04	···	0.92	2.68	···	···	4.5
$L0$	236	−0.02	−0.02	0.85	2.48	0.354	0.71	4.9
$L+$	496	−1.06	2.16	1.04	3.03	0.482	0.96	5.7
$L+$	240	−0.96	2.08	0.97	2.82	0.526	0.94	5.6
$L-$	236	+0.98	−2.54	1.10	3.20	0.622	1.03	6.3
$S0$	507	−0.02	−0.29	2.21	16.9	10.6	1.83	17
$S0$	252	−0.01	−0.77	2.01	16.1	10.7	1.69	27
$S0$	123	−0.03	−0.04	1.88	17.3	11.8	1.84	22
$S0$	59	−0.02	−0.44	2.08	17.5	12.3	2.05	23
$S+\frac{1}{2}$	251	−1.24	9.92	3.44	47.5	46.4	3.56	61
$S+$	252	−3.06	34.3	4.03	62.7	90.0	3.93	76

[a] Average electrical potential (V), field component (E_z), and field gradient component (V_{zz}) and their fluctuations ($\langle \delta V^2\rangle = \langle V^2\rangle - \langle V\rangle^2$ etc.) in atomic units. The data correspond to results of particular simulations as listed in Table IV.

[b] Contributions due to only first solvation shell waters.

ences between the $\langle V\rangle$ values listed in Table VII. We first consider the solvent to be a homogeneous spherical dielectric with radius R and constant ϵ_0. For such a model the reaction potential of an ion of radius r_0 and charge q is

$$V_R(\text{cont}) = \frac{-q}{r_0}\left(1-\frac{1}{\epsilon_0}\right)\left(1-\frac{r_0}{R}\right). \tag{4.2}$$

Figure 7 compares the reaction potentials observed for the ionic solutes to those calculated (X) from Eq. (4.2). For these calculations a value of 218 was used for ϵ_0[61] and the solute LJ radii for r_0. As illustrated by Fig. 7, the simple continuum model does a good job of reproducing the observed potentials, coming within 13% for all of the ions studied. It is surprising that such a crude model should give this level of agreement, especially for the small solutes for which most of the potential comes from about ~7 molecules in the first solvation shell. Also shown in Fig. 7 are the predictions of the MSA model (O), which is based on a dipolar hard-sphere representation of the solvent.[62] This model is of interest, not because it is especially accurate for equilibrium properties[63] but because of its recent extension[26–28] to the dynamical problem to be discussed shortly. The difference between the predictions of the MSA model and the continuum approach can be expressed as

$$V_R(\text{MSA}) = V_R(\text{cont})/(1+\Delta), \tag{4.3}$$

where Δ is a correction term involving the solute/solvent size ratio and ϵ_0. Figure 7 shows that, compared to the simple continuum model, the MSA model yields better agreement to the observed potentials for the large solutes but considerably poorer agreement for the small solutes.

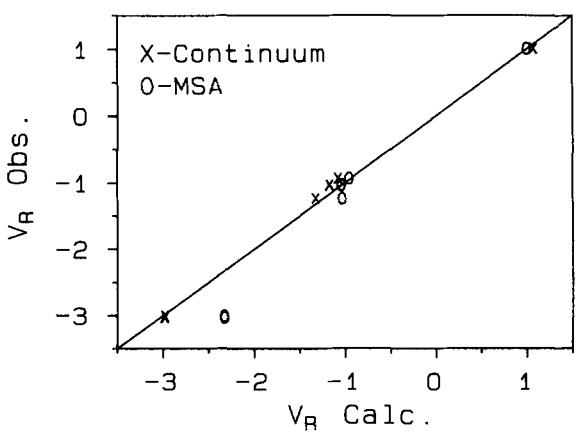

FIG. 7. Observed vs calculated reaction potentials (V_R, a.u.×10) of charged solutes. Observed values are from Table V. Calculated values were obtained for the simple continuum and MSA models using Eqs. (4.2) and (4.3), respectively, as described in the text.

The success of the continuum model for describing the reaction potential does not mean that the polarization surrounding the solute actually looks like that of a continuum fluid. The polarization of a homogeneous spherical continuum surrounding an ion is

$$\mathbf{P}_{\text{cont}}(r) = \frac{-q}{4\pi}\left(1-\frac{1}{\epsilon_0}\right)\frac{\hat{r}}{r^2}. \tag{4.4}$$

In Fig. 8 we plot the ratio of the polarization observed to that calculated on the basis of Eq. (4.4) for two solutes. The actual polarization is highly structured and resembles the water–solute radial distribution functions—quite unlike the simpler r^2 continuum dependence. The molecular, MSA model accounts for just this sort of behavior,[62] so that the reason why the continuum model better reproduces the observed reaction potential is not obvious. We have recently investigated continuum models for solvation dynamics which are based on the idea that the dielectric constant around a solute is not uniform but rather can be characterized by a radially dependent dielectric constant $\epsilon(r)$.[22] We found that for reasonable choices of $\epsilon(r)$ the dynamical predictions of such models closely resemble MSA predictions as well as experimentally observed behavior. The data of Fig. 8 are rather noisy but tend to confirm one important result of that work: the polarization and $\epsilon(r)$ differ substantially from homogeneous continuum predictions only in the region of the first one or two solvation shells. Thereafter, the

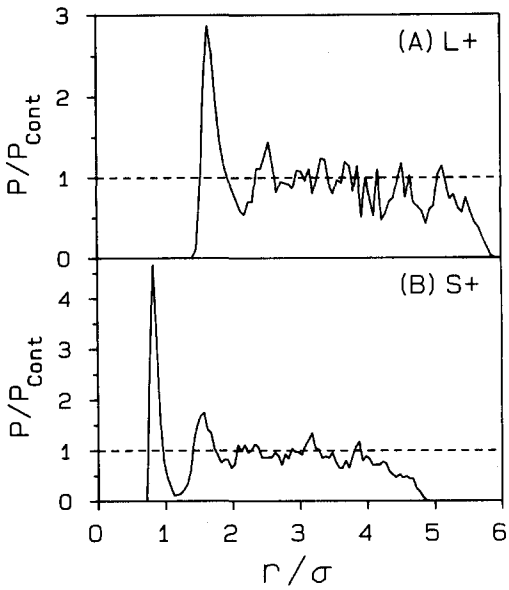

FIG. 8. Solvent polarization surrounding ions (A) $L+$ and (B) $S+$. Radial polarizations ($\Sigma_i \mu_i^* r_i$) were calculated on the basis of point dipoles at the water oxygen positions. The ordinate here is the ratio of the observed polarization to that calculated for a dielectric continuum via Eq. (4.4).

homogeneous continuum description is apt. However, as was previously observed by Chan *et al.*[62] with respect to the MSA model, no $\epsilon(r)$ function everywhere greater than zero is capable of reproducing the highly structured polarization decays observed here. Thus, the present results warn against viewing inhomogeneous continuum [$\epsilon(r)$] models too literally.

V. DYNAMICS FROM EQUILIBRIUM SIMULATIONS

In Sec. IV we discussed the structural features of the first solvation shells of the various solutes. The structure imposed by the solute also alters the translational and rotational dynamics of first solvation shell waters from that of bulk water. This effect is illustrated in Fig. 9 where we have plotted the $l=2$ correlation function of the H–H vector

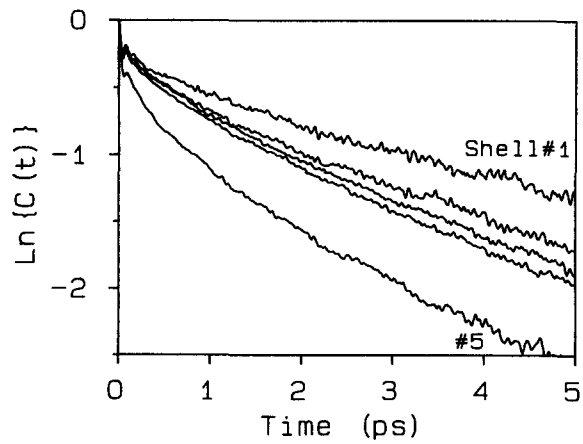

FIG. 9. Reorientational time correlation functions [$C_{2H}(t)$, Eq. (3.1)] of water molecules (512 cluster) as a function of radial shell relative to an $S0$ solute. The shells are defined by the radii (r/σ): 1 = 0–1.60, 2 = 1.60–2.53, 3 = 2.53–3.47, 4 = 3.47–4.40, and 5 = 4.40–6.00.

[$C_{2H}(t)$, Eq. (3.1)] as a function of distance from an $S0$ solute (512 cluster). The average correlation times [Eq. (3.2)] for shells 1–5 are 3.5 (first shell), 2.6, 2.4, 2.2, and 1.4 ps (surface), respectively. The reorientation of waters in the first solvation shell of the $S0$ solute are considerably slower than in the bulk (1.8 ps for pure clusters). The effect of the solute on the dynamics of other shells is small, there being a 25% difference between the average value for interior shells 2–4 of 2.3 ps and the bulk value of 1.8 ps.

Table VI compares the average reorientation times [$C_{2H}(t)$, Eq. (3.1)] in the first solvation shell to the corresponding time in the "bulk" for all solutes studied (256 cluster results). Bulk in this table refers to all waters not in the first solvation shell or in the surface layer. Results for the small solutes are in accord with results obtained previously by a number of groups.[38–40] For both the hydrophobic and hydrophilic extremes represented by $S0$ and $S+$ the reorientation times are roughly 1.5–2 times slower in the first solvation shell than in the bulk. The $S+\frac{1}{2}$ solute exhibits a faster, more bulk-like reorientation time for its first shell waters compared to the $S0$ and $S+$ extremes. This intermediate case is close to the so-called "negative hydration" regime observed experimentally[64] and in computer simulation[38] with ions of small charge/size ratio. In this regime the solute exerts a structure-breaking effect on the first shell water and rotational and translational dynamics are speeded up relative to bulk water. We have previously classified the large solutes as being essentially hydrophobic in character. The 40% slower reorientational correlation times exhibited by $L0$ and $L+$ are in accord with this assignment. The L solute appears to differ from the $L0$ and $L+$ in having a faster first shell correlation time. The cause for such difference is not obvious from the differences in structure. This observation is, however, in agreement with results for other (smaller) anions in ST2 water simulations.[38]

We now consider the time correlation functions that determine solvation dynamics within the linear response approach of Sec. II. These are TCFs of fluctuations in the electrical potential (δV), field (δE_z), and field gradient (δV_{zz}) at the solute center and they correspond, respectively, to solvation responses to step changes in the magnitude of a centered point charge, dipole, or quadrupole as described by Eq. (2.10). Figure 10 displays these three correlation functions observed with the $S0$ and $S+$ solutes. Figure 11 and Tables VII and VIII summarize the results for all of the solutes studied. The data and error bars shown in Fig. 10 are representative of the results of these simulations. All three correlation functions contain a very fast ($\sim$25 fs) component that accounts for more than half of the total decay. This component is a result of librational motions of water molecules.[65] We note that the presence of such a large amplitude, fast component may be of prime importance in understanding reactions with high reactive frequencies in water. A longer component, which decays on a 1 ps time scale, is a result of diffusive reorientations, and in some cases translational motions of solvent molecules (see below). For the $S0$ molecule [Fig. 10(A)] the decay of the potential TCF, $\langle \delta V \delta V(t) \rangle$, is the most rapid with the relative ordering being given by $\delta V > \delta V_{zz} > \delta E_z$. With the exception of the $S+$ solute

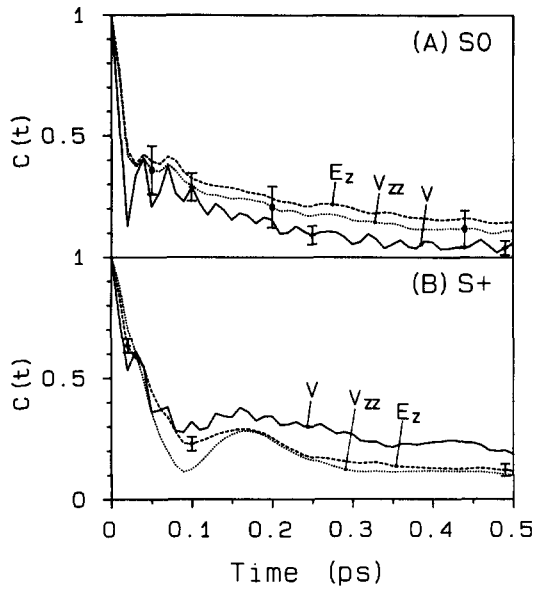

FIG. 10. Time correlation functions of electrical properties observed for solutes (A) $S0$ (B) $S+$ (256 clusters). The three curves in each panel correspond to the normalized TCFs: solid = $\langle \delta V \delta V(t) \rangle$; dashed = $\langle \delta E_z \delta E_z(t) \rangle$; and dotted = $\langle \delta V_{zz} \delta V_{zz}(t) \rangle$. Error bars are estimates of the statistical uncertainty due to finite simulation length.

shown in Fig. 10(B), for which δV decayed the most slowly, the $S0$ ordering is consistently observed for the remaining solutes. In addition to its faster decay, in most cases the $\langle \delta V \delta V(t) \rangle$ TCFs also show pronounced librational oscillations,[67] largely absent in the $\langle \delta E_z \delta E_z(t) \rangle$ and $\langle \delta V_{zz} \delta V_{zz}(t) \rangle$ TCFs [Fig. 10(A)]. We will discuss reasons for this behavior in Sec. VI.

Before discussing the dynamic differences observed for the various solutes we first ask how the finite samples presented by these clusters might affect our results. It is useful to calibrate expectations by again considering a continuum

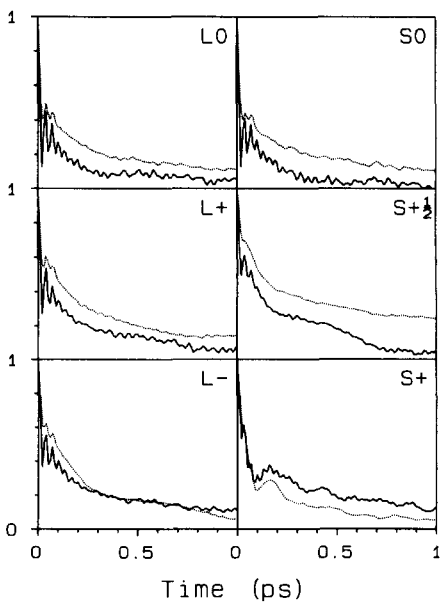

FIG. 11. Summary of the time correlation functions $\langle \delta V \delta V(t) \rangle$ (solid curves) and $\langle \delta E_z \delta E_z(t) \rangle$ (dotted) for all solutes studied (256 clusters).

TABLE VIII. Time constants of electrical TCFs.[a]

Solute	N_{solv}	$\langle \delta V \delta V(t) \rangle$	$\langle \delta E_z \delta E_z(t) \rangle$	$\langle \delta V_{zz} \delta V_{zz}(t) \rangle$
$L0$	496	0.07	0.14	···
$L0$	236	0.11	0.19	0.13
$L+$	496	0.14	0.17	0.14
$L+$	240	0.16	0.25	0.22
$L-$	236	0.21	0.21	0.19
$S0$	507	0.12	0.18	0.15
$S0$	252	0.09	0.16	0.14
$S0$	123	0.10	0.17	0.14
$S0$	59	0.09	0.10	0.08
$S+\frac{1}{2}$	251	0.20	0.33	0.30
$S+$	252	0.23	0.15	0.13

[a] Approximate time constants (ps) of the TCFs of the electrical potential, field, and field gradient fluctuations [Eq. (2.10)]. These times are integrals of the normalized correlation functions between 0 and 1 ps. The correlation functions have not decayed completely to zero so that the values listed are lower limits to the average time constants.

dielectric sphere as a model. The interaction energies of point ion, dipole, and quadrupole solutes of radius r immersed in such a sphere having radius R are related to their energies in an infinite medium by the fractions $[1 - r/R]$, $[1 - (r/R)^3]$, and $[1 - (r/R)^5]$. On this basis, Table V lists values of the percentage of the bulk response expected missing from cluster simulations using 64 to 512 molecule clusters and the two solute sizes under study. Most of our comparisons are based on 256 clusters. For such clusters, Table V indicates that we miss ~13% and ~29% of the ionic solvation energy of S and L size solutes, respectively. For the ionic case, these values do not improve markedly upon increasing the cluster size to 512. Solvation of the higher order multipoles are predicted to be much less influenced by sample size. According to Table V, less than 3% of the total dipolar solvation energy is neglected in 256 clusters, and for quadrupole solvation the missing energy is at most 0.2%. Even for the worst case of an L solute in a 64 molecule cluster the continuum approach predicts that at least 90% of the full dipolar solvation energy should be accounted for. From this exercise we conclude that our cluster results for ion solvation dynamics may be somewhat influenced by the sample sizes used. Deviations from the dynamics occurring in bulk solution could be substantial for the large solutes but should be quite small for the small solutes. Sample size probably has little observable effect on the calculated dipolar and quadrupolar solvation dynamics.

Comparisons of the simulation results in Tables VII and VIII for the same solute in different size clusters tends to confirm the above expectations. In Table VII we list the amplitudes $\langle \delta V^2 \rangle$, $\langle \delta E_z^2 \rangle$, and $\langle \delta V_{zz}^2 \rangle$ of the electrical properties. These $t = 0$ amplitudes determine the total change in solvation energy in response to the three multipole jumps. Given that the statistical uncertainties in these quantities are all in the range 5%–10% it is difficult to say with confidence that differences as a function of cluster size, which are typically less than 10%, are significant. The approximate time constants for decay of these TCFs, listed in Table VIII, show much larger dependence on cluster size than do the amplitudes. Taking into account the roughly ± 30% uncertainties in these times, there still appears to be a significant differ-

ence between the dynamics of L solutes in 256 and 512 clusters. For L 0 and L + all three correlation functions decay consistently faster in the larger size cluster. Based on the continuum arguments given above, such behavior is not surprising for the $\langle \delta V \delta V(t) \rangle$ correlation function. However, observing an apparently larger effect on the $\langle \delta E_z \delta E_z(t) \rangle$ and $\langle \delta V_{zz} \delta V_{zz}(t) \rangle$ TCFs is unexpected. The direction in which the rates change, getting faster with increased cluster size, is consistent with current understanding of the solvation response (see below). In contrast to the L solutes, the series of S0 solute simulations shows little systematic variation of decay time with cluster size. The one exception is the 59 molecule cluster, which is actually too small to achieve bulk-like behavior. (For this size cluster nearly all molecules are part of the surface layer and the density, orientational distributions, and reorientation times in even the first solvation shell are substantially different from their values in larger clusters. Thus, agreement with the larger cluster results is not expected in this case and the simulation was run merely to gauge how large the differences would be.) To summarize, we find that the dynamics calculated for the large solutes with clusters of size 256 and even 512 may differ significantly from the bulk dynamics. Without performing larger simulations it is difficult to assess the magnitude of this effect, however, it seems unlikely that the time constants we observe would differ from the infinite size limit by more than a factor of 2. The small solutes do not seem to be sensitive to size effects for clusters in the range studied; thus, our observations for these solutes should directly reflect bulk dynamics.

Figure 11 illustrates the differences in solvation dynamics observed among the different solutes in clusters of size 256. For clarity we have only plotted the electrical potential and field correlation functions. With the exception of S +, the field gradient correlation function lies between the two TCFs that are plotted here. (The δV_{zz} TCF is also generally similar in appearance to the δE_z correlation function, as illustrated in Fig. 10.) Uncertainties in these $C(t)$ plots are all similar to those provided in Fig. 10. The time constants listed in Table VIII serve to quantify the differences in the overall decay times of these correlation functions. These times are calculated as the integral under the $C(t)$ curves as in Eq. (3.2) except that the integration is only carried out to $t = 1$ ps rather than to infinity in order to avoid the large errors incurred by further integration. As can be seen from Fig. 11, most of the $C(t)$ curves have not decayed to zero by this time and thus the values listed in Table VIII, although useful for comparison purposes, are only lower limits to the actual time constants of these correlation functions.

The main differences in the dynamics among the different solutes are as follows. The time constants of the uncharged solutes L 0 and S0 are the same to within estimated uncertainties, and the shapes of all three TCFs are also indistinguishable. (The amplitudes of the fluctuations, listed in Table VII, are of course larger for the small solute.) Thus, a factor of 2.25 in the solute/solvent size ratio has no observable effect on the solvation dynamics. We note that the similarity between S0 and L0 tends to argue against cluster size appreciably affecting even the L solute results. The $\langle \delta V \delta V(t) \rangle$ correlation functions decay more slowly in the charged solutes relative to the uncharged solutes. This is also true of the $\langle \delta E_z \delta E_z(t) \rangle$ and $\langle \delta V_{zz} \delta V_{zz}(t) \rangle$ functions except in the S + case. It is somewhat surprising that the solvation dynamics for L + and L − should differ significantly from that of L0 since their solvation structures are so similar. In fact, rather subtle differences in the structure about L0, L +, and L − appear to be responsible for the different dynamics. For the large charged solutes we observe that a small fraction (~4 out of 40) of the nearest-neighbor solvent molecules are persistently oriented so as to point an appropriately charged interaction site at the solute. The dynamics of these particular waters is slower than the "normally" oriented waters and this seems to account for the difference in dynamics compared to the uncharged case. All solvation TCFs of small charged solute $S + \frac{1}{2}$ decay much more slowly than those of its uncharged counterpart. The dependence of response time on charge is not simple however, and the more highly charged S + shows a similar response time for the potential TCF but times for the field and field gradient TCFs which are as fast as in the uncharged solute. As we have already described, the environment surrounding these small solutes changes appreciably as a function of charge so that such differences in dynamics are to be expected. Some explanation for these differences will be discussed in Sec. VI. For now we note that the variations in the collective TCFs do not correlate with the single particle reorientation times given in Table VI.

It is useful to compare our results with the one published study that provides the same sort of dynamical information as derived here.[68] In their MD simulations of quadrupolar NMR relaxation, Engström *et al.*[44] calculated the $\langle \delta V_{zz} \delta V_{zz}(t) \rangle$ correlation functions of Li^+, Na^+, and Cl^- ions in MCY[69] water. From their data we estimate average decay times of $\geqslant 0.16$, > 0.25, and > 0.47 ps for these three ions, respectively. None of our solutes have interaction parameters that correspond closely to any of these ions, however, based on solute–oxygen radial distribution functions, we find that the size of Na^+ is just slightly smaller than our S + solute. The value of > 0.25 ps for Na^+ may thus be compared to our value of > 0.13 ps for S +. On this basis we conclude that the two simulations are not in quantitative agreement. The qualitative features of the $C(t)$ decays reported by Engström *et al.* are, however, consistent with our findings. For example, the correlation functions observed for Li^+, Na^+, and Cl^- all show a very rapid (~25 fs) decay to less than half of the $t = 0$ value, and then a slower decay with time constant somewhere in the few hundred fs range. The trend of decreasing decay time with increasing charge to size ratio is also in keeping with our findings for $S + \frac{1}{2}$ and S +. Lack of quantitative agreement between the two sets of results can probably be attributed to differences in the water models used. Engström *et al.* performed several of the above simulations with varied system sizes of 64 and 125 molecules, and used both periodic (Ewald) and free cluster boundary conditions. Since no significant difference in the $\langle \delta V_{zz} \delta V_{zz}(t) \rangle$ TCFs was observed due to these variations it is unlikely that our two simulations would differ due to such effects. On the other hand, characteristics of the two water

models are significantly different. The dipole reorientation time of the MCY water model[70] is 2–3 times faster than the ST2 value. Furthermore, the placement and magnitude of negative charges in these models is quite different, which would be expected to have a significant effect on the solvation of positively charged ions. Thus, the quantitative differences observed with these two water models are not surprising. Since we do observe this model dependence, caution should be exercised in assuming that either sets of results provide more than a semiquantitative guide to the behavior of real water.

VI. COMPARISON TO THEORETICAL PREDICTIONS: MOLECULAR ASPECTS

In this section we compare the solvation dynamics calculated from equilibrium simulations under the linear response assumption to predictions of two theoretical treatments. The first theory is the dynamic extension[8–12] of the simple continuum model we have already used several times for discussing the static energetics. This model treats the solvent as a continuum dielectric fluid that is characterized by its bulk dielectric dispersion, $\epsilon(\omega)$. The onset of a bulk $\epsilon(\omega)$ is assumed to occur abruptly at the boundary of the solute, and thus the simple continuum model completely ignores any effects that the molecular nature of the solvent might have on the dynamics. The second and more recent approach, the dynamical MSA model,[21,26–28] does consider molecular effects through use of a hard-sphere solute and a dipolar hard-sphere solvent as a reference system. The static behavior of such a model system can be solved within the mean spherical approximation (MSA) and can then be used to predict solvation dynamics for a real solvent. Loosely speaking, the dynamics are obtained by replacing ϵ_0 in the static reference model by $\epsilon(\omega)$ of the solvent of interest. Predictions of the dynamical MSA model depend on $\epsilon(\omega)$ and, in addition, on the single molecular parameter ρ, the ratio of the solvent and solute sizes.

In order to compare the predictions of these two models to our simulation results, the dielectric dispersion of the ST2 water model is needed. In the Appendix we describe an approximate cluster calculation of $\epsilon(\omega)$. Here we will use preliminary results of an extensive investigation by Neumann[61] since these should be more accurate. Neumann's results (293 K) can be expressed in terms of a triple Debye fit as

$$\epsilon(\omega) = \epsilon_{\infty 3} + \sum_{j=1}^{3} \frac{\epsilon_{0j} - \epsilon_{\infty j}}{1 + i\omega\tau_{Dj}} \tag{6.1}$$

using the parameters

$$\epsilon_0 = \epsilon_{01} = 218, \quad \tau_{D1} = 33.16 \text{ ps},$$
$$\epsilon_{\infty 1} = \epsilon_{02} = 2.73, \quad \tau_{D2} = 0.177 \text{ ps},$$
$$\epsilon_{\infty 2} = \epsilon_{03} = 1.79, \quad \tau_{D3} \cong 0.013 \text{ ps},$$
$$\epsilon_{\infty} = \epsilon_{\infty 3} = 1.$$

In this expression we have approximated the librational resonance observed by Neumann ($\omega \sim 2\times 10^{14}\,\mathrm{s}^{-1}$) in terms of a third relaxation regime in order to simplify the theoretical calculations. The main effect of such an approximation is to smooth out any oscillatory behavior in the calculated response without significantly changing its overall shape except at very early times. The dielectric constant of ST2 water is much too high compared to the experimental value of 78.4 (298 K, Ref. 57), in keeping with the general observation that ST2 water tends to overestimate the extent of ordering present.[30] The Debye time of the main dispersion τ_{D1} is also quite long compared to the experimental value of 8.3 ps.[57] However, the quantities of most relevance for solvation dynamics are the longitudinal relaxation times. For the main (1) dispersion regime, the longitudinal relaxation time $[\tau_{L1} = (\epsilon_{\infty 1}/\epsilon_{01})\tau_{D1}]$ of this model is 0.42 ps (or 0.49 ps[71]) compared to an observed value of 0.54 ps. Thus, although the ST2 potential yields rather poor estimates of ϵ_{01} and τ_{D1}, predictions of solvation dynamics based on this model are expected to be much more accurate.

Figure 12 illustrates the solvation response functions $S(t)$ calculated from the simple continuum, and dynamical MSA models using the above $\epsilon(\omega)$. In Fig. 12(A) the response to a change in solute charge, i.e., the $\langle \delta V \delta V(t) \rangle$ response, is shown. The simple continuum model predicts a response that is independent of solute size or charge. The MSA prediction does depend on the solvent/solute size ratio and the two curves shown correspond to values approximate to S and L solutes as marked. All three $S(t)$ curves exhibit a fast initial decay that arises from the librational (τ_{D3}) component of $\epsilon(\omega)$. The longer time part of $S(t)$ is due to the true relaxation terms (τ_{D1}, τ_{D2}). Within the simple continuum model these two dispersions produce a biexponential $S(t)$ which after $\sim$0.5 ps becomes nearly monoexponential with a time constant of 0.49 ps. In contrast, the $S(t)$ curves predicted by the MSA model are nonexponential over the time window shown, and decay much more slowly than the continuum model. These features are characteristic of the

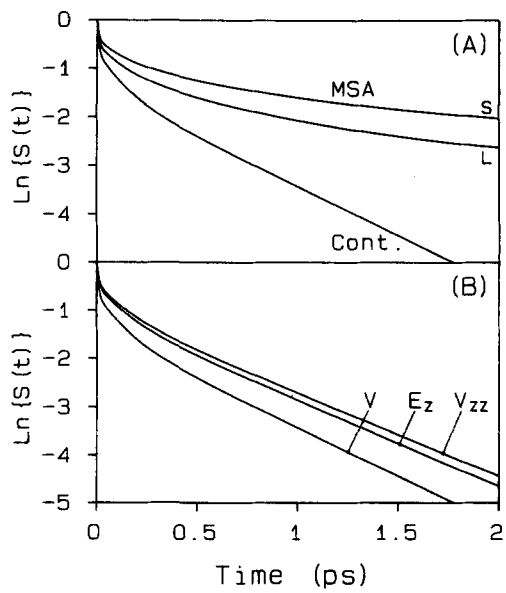

FIG. 12. Solvation responses functions predicted by the continuum and MSA models (see the text). (A) Response to a step function change in solute charge. The MSA prediction depends on solute size and the curves labeled S and L correspond to the two solute sizes simulated. (B) Responses to step function changes in solute charge (V), dipole moment (E_z), and quadrupole moment (V_{zz}) predicted from the continuum model. These $S(t)$ curves are labeled according to the equilibrium TCFs to which they correspond according to Eq. (2.10).

predictions of the MSA model even for single Debye $\epsilon(\omega)$. The average time constants [Eq. (3.2)] of the three curves in Fig. 12(A) are: simple continuum $\langle\tau\rangle = 0.15(0.13)$ ps, MSA L $\langle\tau\rangle = 0.94(0.24)$ ps, and MSA S $\langle\tau\rangle = 1.7(0.33)$ ps. The numbers in parentheses are the values obtained when the integral over $S(t)$ is truncated at 1 ps, and are given for comparison with the simulation results listed in Table VIII.

Figure 12(B) shows the continuum model predictions for the response to jumps in a solute's charge, dipole moment, and quadrupole moment. The continuum model predicts that the solvation times increase in the order ion < dipole < quadrupole with average response times [Eq. (3.2)] of 0.15, 0.23, and 0.25 ps, respectively. The long time behavior of all three of these responses is similar; the limiting slopes in Fig. 12(B) give time constants of 0.49, 0.55, and 0.57 ps. The same relative ordering of response times should also hold for the dynamical MSA model, however, the differences between the multipoles are predicted to be larger. Unfortunately, the dynamical MSA model has not been solved for higher multipoles with arbitrary $\epsilon(\omega)$ except in the case of a dipolar solute of size equal to that of the solvent.[27(b),72] For the one available comparison, that of a dipolar jump in an S solute, the MSA model[24(b)] predicts $\langle\tau\rangle = 5.1(0.63)$ ps compared to the 1.7(0.33) ps for a charge jump.

In Fig. 13 we plot the simulated $C(t)$ TCFs in the same manner as the theoretical predictions. In order to obtain the best signal to noise in these logarithmic plots we have averaged together results of several simulations. Since the uncharged solutes L 0 and S 0 exhibit $C(t)$'s that are identical to within our uncertainties, we combined results of these solutes in producing Fig. 13. $\langle\delta V\delta V(t)\rangle$ correlation functions, to be compared with the ionic $S(t)$'s in Fig. 12(A), are shown for the solutes S 0/L 0, L +, and S + in Fig. 13(A). One point, which was obvious even before carrying out the

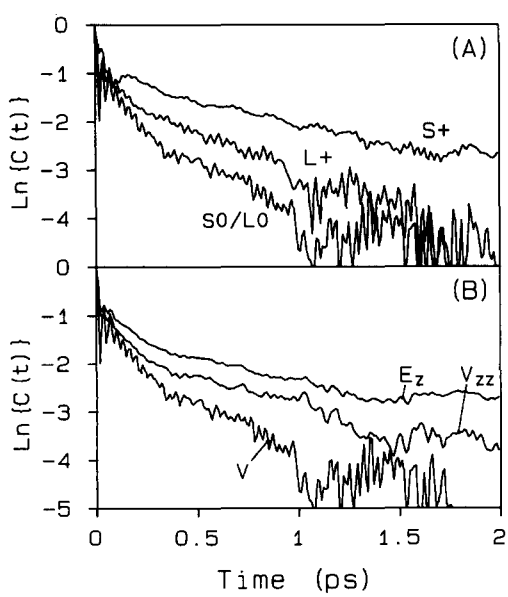

FIG. 13. Electrical time correlation functions observed for several solutes plotted for comparison to the theoretical predictions in Fig. 12. (A) $\langle\delta V\delta V(t)\rangle$ TCFs for solutes S +, L +, and S 0/L 0. These curves were obtained by averaging results of several simulations. For the S 0/L 0 curve results for S 0 and L 0 solutes were combined. (B) $\langle\delta V\delta V(t)\rangle$, $\langle\delta E_z\delta E_z(t)\rangle$, and $\langle\delta V_{zz}\delta V_{zz}(t)\rangle$ TCFs for S 0/L 0 solutes.

theoretical calculations, is that neither model is able to account for the variations we see in the $\langle\delta V\delta V(t)\rangle$ TCFs of the different solutes. The simple continuum model predicts that $\langle\delta V\delta V(t)\rangle$ (and the other TCFs) should be the same for all solutes. In fact, we observe that they decay with time constants that differ several fold. The dynamical MSA model does allow for some differences in the behavior of different solutes but the only solute attribute accounted for is size. In contradiction to the MSA prediction [Fig. 12(A)], we find that over the range used here, size is of little importance. It is rather the charge/size ratio that appears to determine the dynamical differences seen among these solutes. With this underlying difficulty in mind, we note that $\langle\delta V\delta V(t)\rangle$ of the uncharged solutes is close to the prediction of the simple continuum model, except for being slightly faster at early times. The dynamical MSA model predicts decays that are too slow compared to any of the observed $\langle\delta V\delta V(t)\rangle$ TCFs. Figure 13(B) illustrates the observed ordering of the potential, field, and field gradient TCFs using the uncharged solutes as an example. Although the potential TCF does decay the most rapidly, as predicted by both theories, the ordering of the other two TCFs is reversed from that predicted. The long time behavior of the $\langle\delta E_z\delta E_z(t)\rangle$ and $\langle\delta V_{zz}\delta V_{zz}(t)\rangle$ TCFs is slower than that of $\langle\delta V\delta V(t)\rangle$ or the predictions of the continuum model and approaches the sort of decays predicted by the MSA theory. However, no TCFs were observed to decay as slowly as the MSA dipole prediction (not shown).

To summarize, neither the simple continuum model nor the dynamical MSA model is able to quantitatively reproduce the observed behavior. The best that can be said is that the predictions of overall time scales appear to be within about a factor of 2 or 3 of the observed values. The reasons for lack of predictive ability of these theories arises, at least in part, from the highly structured nature of aqueous solvation. We now investigate some of the dynamical consequences of this structure.

In Fig. 14 we consider how the total solvation response is built up from contributions of different solvent regions. In this figure we concentrate on the response to a change in solute charge as determined by the $\langle\delta V\delta V(t)\rangle$ correlation function. For an example we will use the results of a simulation of the S 0 solute in a 256 cluster, however, our observations are general. In Fig. 14(A) we plot contributions to $\langle\delta V\delta V(t)\rangle$ from a series of shell regions 1–3 whose definitions are provided in Table IX. Also shown in Fig. 14(A) is the single particle reorientational TCF of the dipole moment direction [$C_{1d}(t)$, Eq. (3.1)] for molecules in the first solvation shell. The contribution made by any one molecule to $\langle\delta V\delta V(t)\rangle$ decays on a time scale similar to this reorientational TCF.[73] The difference between the decay times of $\langle\delta V\delta V(t)\rangle$ and this single particle time is striking and serves to highlight the fact that the solvation response is as fast as it is because it results from the concerted motion of many molecules. The number of molecules actually required to achieve the full cooperativity of the response appears to be of order 10–40, based on the fact that both the first and second shells exhibit this fast decay. A second important feature illustrated by Fig. 14(A) is how important the first shell

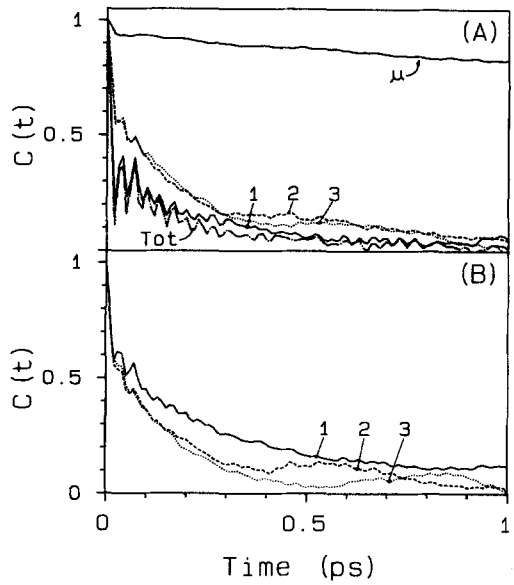

FIG. 14. Electrical time correlation functions for an $S0$ solute decomposed into individual shell contributions. (A) $\langle \delta V \delta V(t) \rangle$. The solid curve at the bottom is the total TCF and the curves labeled 1–3 are the contributions of individual shells 1–3. (Definitions of the shell regions are provided in Table IX.) The curve marked μ is the single-particle dipole TCF [$C_{1d}(t)$, Eq. (3.1)] shown for comparison. (B) Correlation functions of the radial polarizations [P_r, Eq. (6.2)] of the shell regions.

contribution is to the total response. The $t = 0$ amplitude ($\langle \delta V^2 \rangle$) contributed by the first solvation shell is 85% of the total (see Table VII). Furthermore, the large oscillations as well as the rapid decay of the potential TCF are due predominantly to the behavior of first shell molecules. For the $S0$ solute the first shell contains ~ 16 molecules. If one examines the potential correlation function for only half this number of first shell molecules, the oscillations as well as the rapidity of the response decrease markedly. Thus, both effects appear to be a collective libration of all molecules in the first solvation shell.

A further aspect of the first shell contribution is that it is sensitive to the finite size of the solvent molecules in a way not reflected in $\epsilon(\omega)$. The dielectric response of a liquid depends only on reorientational dynamics of the molecular dipole moment. To the extent that this is also true of the $\langle \delta V \delta V(t) \rangle$ TCF, the shell contributions to $\langle \delta V \delta V(t) \rangle$ should be related to the shell polarizations as

$$\frac{\langle \delta V \delta V(t) \rangle}{\langle \delta V^2 \rangle} \cong \frac{\langle \delta P_r \delta P_r(t) \rangle}{\langle \delta P_r^2 \rangle}, \tag{6.2}$$

where P_r is the radial component of the polarization

$$P_r = \sum_j \boldsymbol{\mu}_j \cdot \hat{\mathbf{r}}_j \tag{6.3}$$

of a shell. [The summation in Eq. (6.3) extends only over molecules in a given radial shell.] Figure 14(B) shows the polarization TCFs as a function of shell for the same $S0$ simulation as in Fig. 14(A). In contrast to $\langle \delta V \delta V(t) \rangle$, the $\langle \delta P_r \delta P_r(t) \rangle$ TCF of first shell waters actually decays more slowly than the other shells. Note also that the first shell polarization shows little of the oscillatory behavior of the potential TCF. The second and third shell polarizations decay with essentially the same time dependence as their contributions to $\langle \delta V \delta V(t) \rangle$. This latter observation is to be expected since, except for the innermost shell, interactions between the solute and solvent should be well represented treating the solvent as point dipoles. Lack of agreement between $\langle \delta P_r \delta P_r(t) \rangle$ and $\langle \delta V \delta V(t) \rangle$ in the first solvation shell indicates that here the solute does not view solvent molecules as simple point dipoles but rather interacts with their extended charge distribution, in this case the four point charges of the ST2 model. A second cause for the difference could also be that translational motions of molecules in the first shell significantly contribute to the response. That is since $V \propto P_r/r$, changes in r as well as changes in P_r can affect the $\langle \delta V \delta V(t) \rangle$ decay. As will be discussed presently this latter effect appears to be small on the potential TCFs of uncharged solutes.

Figure 15 illustrates the shell contributions to the elec-

TABLE IX. Shell definitions used in $S0$ and $S+$ simulations.[a]

Shell No.	r_{in}[b]	r_{out}[b]	No. mols[c]
	$S0$ solute		
1	0	1.60	16.4
2	1.60	2.45	43.4
3	2.45	3.30	83.1
4	3.30	5	109.1
	$S+$ solute		
1	0	1.10	6.9
2	1.10	2.20	39.4
3	2.20	3.30	101.8
4	3.30	5	103.8

[a] 256 molecule clusters.
[b] Inner and outer shell boundaries in units of the ST2 σ.
[c] Average numbers of molecules in shell.

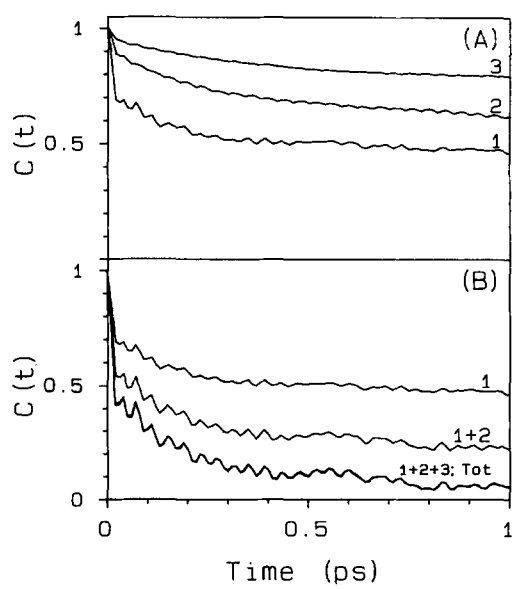

FIG. 15. Shell contributions to the $\langle \delta E_z \delta E_z(t) \rangle$ TCF of an $S0$ solute: (A) individual shell contributions and (B) sums over individual shell contributions. Note that in panel (B) there are two curves at the bottom of the plot that are nearly superimposed—that of the $\langle \delta E_z \delta E_z(t) \rangle$ contribution from regions 1–3 and that of the total (1–4) TCF. Definitions of the shell regions are provided in Table IX.

tric field TCF, $\langle \delta E_z \delta E_z(t) \rangle$, for the same $S0$ simulation. The contrast between the behavior of this field correlation function and the potential or polarization TCFs just discussed is remarkable. As seen from Fig. 15(A), after an initial fast librational decay, the contributions from any given shell decay very slowly. It is only when contributions of successive shells are summed [Fig. 15(B)] that the response achieves the very fast rate characteristic of solvation. Such a difference between the behavior of the potential and field TCFs is surprising. At first sight, it appears that to obtain the fast solvation response many more molecules are required in the $\langle \delta E_z \delta E_z(t) \rangle$ TCF than in the $\langle \delta V \delta V(t) \rangle$ TCF. Since the range of the field is much smaller than that of the potential, this result is counter intuitive. The problem is in some sense an artifact and involves the difference between the scalar and vector character of V and $\mathbf{E}$. We note that the way in which the shell contributions to $\langle \delta E_z \delta E_z(t) \rangle$ decay is sensitive to the exact placement of the shell boundaries, a feature not observed for $\langle \delta V \delta V(t) \rangle$. What causes this sensitivity is the fact that solvent molecules are not spherically distributed about the solute. For a shell of molecular width, at any given time one is likely to find, e.g., an "extra" solvent molecule present in the $+z$ direction as compared to the $-z$ direction. The electric field produced by molecules in this shell, especially the E_z component, will notice this directional asymmetry. The potential, on the other hand, will only be sensitive to the net number of molecules in the shell and not to any directional biasing. It seems reasonable to assume that the spherically averaged density of a shell should fluctuate less, and on a faster time scale than fluctuations at any particular point within the shell which should proceed on a diffusional time scale. Thus, shell contributions to $\langle \delta E_z \delta E_z(t) \rangle$ include components due to relatively slow diffusion in and out of the shell regions much more so than does the spherically averaged $\langle \delta V \delta V(t) \rangle$ TCF. Only when these diffusional components are suppressed by summing shells together (i.e., making them larger) are decays similar to the $\langle \delta V \delta V(t) \rangle$ shell contributions obtained. The above arguments would imply that the shell contributions to $\langle \delta V_{zz} \delta V_{zz}(t) \rangle$ should probably be more similar to the $\langle \delta E_z \delta E_z(t) \rangle$ TCFs than to those of $\langle \delta V \delta V(t) \rangle$. Unfortunately, we do not have such data available for the field gradient components.

The last aspect of the equilibrium TCFs that we will consider is the molecular basis for the differences observed among the charged and uncharged solutes. We first note, as expected, these differences are due almost entirely to differences in first solvation shell dynamics. For example, the potential and polarization TCFs of $S0$ and $S+$ are the same to within uncertainties for all but the first solvation shell. Figures 16 and 17 contrast the behavior of molecules in the first solvation shells of $S0$ (Fig. 16) and $S+$ (Fig. 17) solutes. What are plotted here are three observables of the trajectories of a single solvent molecule. In both figures panel (A) shows the solute–oxygen distance, panel (B) the cosine of the angle between the solvent dipole and the radius vector, and panel (C) the single-molecule contribution to the electrical potential at the solute center. Comparison of panels (A) and (B) on either figure shows that small scale rotational motions occur with roughly four times the frequency of translational motions.[74] These two motions contribute with different weights to the potential fluctuations in the two solutes and are responsible for the differences between their $\langle \delta V \delta V(t) \rangle$ decays. For the $S0$ solute, Fig. 16 shows that fluctuations in the potential [Fig. 16(C)] arise mainly from rotational motions, overall molecular translation has little affect on the potential. This is not the case for the $S+$ solute for which translational motions do play an important part in the potential fluctuations. Waters in the first solvation shell of $S+$ point one of their negative charges (Q_1) directly at

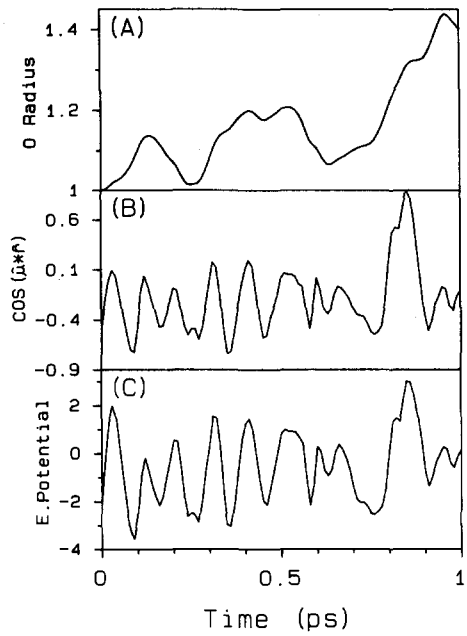

FIG. 16. Properties of the trajectory of a single solvent molecule in the first shell of an $S0$ solute: (A) solute–oxygen distance; (B) $-\cos(\hat{\mu}^*\hat{r})$ where $\hat{\mu}$ is the dipole direction and $\hat{r}$ the solute–oxygen vector; and (C) the single-molecule contribution to the electrical potential.

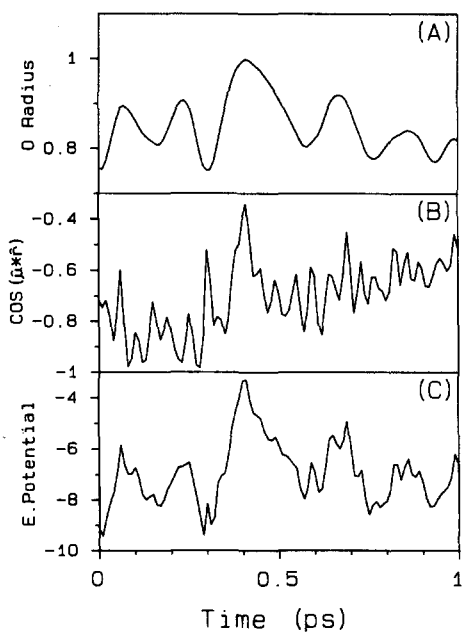

FIG. 17. Properties of the trajectory of a single solvent molecule in the first shell of an $S+$ solute (see caption to Fig. 16).

the solute and are held rather tightly. The tight binding is manifest in the coherent vibrational character of the solute–oxygen distance shown in Fig. 17(A). [This coherence is also responsible for the unique oscillation at ~0.18 ps in the $S+$ TCFs shown in Fig. 10(B).] In the "pointing" configuration, Q_1 is close to the solute center, and it is mainly the solute-Q_1 distance that determines the potential. Fluctuations in this distance result primarily from translational (/vibrational) motions rather than rotational motions as is illustrated in Fig. 17. That is, while the rapid spikes in Fig. 17(C) do come from motions that are rotational in character, the overall contour of the potential trajectory closely matches excursions in the oxygen (essentially the center of mass) to solute distance. Thus the much slower $\langle \delta V \delta V(t) \rangle$ response of the $S+$ solute compared to the $S0$ solute is a result of the importance of slower, translational mechanisms of relaxation in the former and not the latter solute.

The observations made on the basis of Figs. 16 and 17 can be generalized to the other solutes and responses. As expected, the large uncharged solute behaves in much the same way as does $S0$. The $S+\frac{1}{2}$ solute seems to have important contributions from both rotational and translational mechanisms. As already discussed, the first shell structure surrounding this solute is a mix of the structures observed for $S0$ and $S+$. The fraction of nearest neighbors in the pointing configuration contribute to the decay of $\langle \delta V \delta V(t) \rangle$ mainly via their translational dynamics whereas the other first shell solvents appear to have mainly rotational contributions. The case for the $L+$ and $L-$ solutes is similar although less clear cut. We do observe that a small fraction of the nearest neighbor molecules of these solutes adopt pointing configurations. These molecules appear to be responsible for the slower overall response, however, it is difficult to say that they contribute mainly via a translational mechanism, since with the large solutes the effect is considerably blurred, and reorientational motions are equally important.

We have also investigated how the single-molecule dynamics affect the higher order, $\langle \delta E_z \delta E_z(t) \rangle$ and $\langle \delta V_{zz} \delta V_{zz}(t) \rangle$ TCFs. Comparisons like those shown in Figs. 16 and 17 for the potential are similar in these latter cases. One difference is that there is a less direct relation between fluctuations in the field and field gradient and the dipole angle for $S0$ than is shown in Fig. 16. Since solvent molecules are not point dipoles, the dipole direction only partially specifies the electrostatic interaction with the solute for small separations. (This effect is responsible for the difference between the polarization and potential TCFs described earlier.) The difference should be least important for the potential and become progressively more noticeable for the progressively shorter range field and field gradient properties. Thus the above observation is to be expected. For the same reasons we would anticipate translational effects to become of increasing importance in this same order. This expectation does seem to be born for the $S+$ solute where, e.g., we observe that the low-frequency oscillations in the solvation time correlation functions caused by translational motions increase in amplitude in the order $\langle \delta V \delta V(t) \rangle < \langle \delta E_z \delta E_z(t) \rangle < \langle \delta V_{zz} \delta V_{zz}(t) \rangle$ [Fig. 10(B)]. The high-frequency oscillations in these TCFs, due to librational dynamics, decrease for all solutes in this same order. Thus, it appears that differences in the three multipole response functions, which parallel the differences observed in $\langle \delta V \delta V(t) \rangle$ in the progression $S0 \rightarrow S+\frac{1}{2} \rightarrow S+$, may also reflect the increasing relative importance of translational relaxation mechanisms.

VII. NONEQUILIBRIUM SIMULATIONS

In Secs. V and VI, we have examined the time dependence of the solvation response using results of equilibrium MD simulations. The TCFs of electrical properties observed in equilibrium are simply related to the nonequilibrium solvation response [via Eqs. (2.10)] only to the extent that the linear response approximation is valid. Thus, if an $S0$ solute in equilibrium is suddenly given an increment of charge δq, the subsequent relaxation of the solvation energy follows the same time dependence as $\langle \delta V \delta V(t) \rangle$ evaluated with $S0$ in equilibrium, *as long as δq is sufficiently small.* The question remains as to just how small the charge (or dipole, or quadrupole) change must be for the linear response approximation to hold good. In Sec. IV we observed that the static energies of solvation of ions behaved in a linear manner over an unexpectedly large range of charge. In order to explore what happens for the dynamics, we have performed a number of nonequilibrium simulations in which we directly monitor the solvation response to a change in solute charge. The charge jumps we simulated are listed in Table I and correspond to changes among the various solutes that were studied in equilibrium. From such simulations we derive the normalized function $S(t)$ of the electrical potential $[V(t)]$ response to the jump (at $t=0$):

$$S(t) = \frac{V(t) - V(\infty)}{V(0) - V(\infty)}. \tag{7.1}$$

Comparison of $S(t)$ to the $\langle \delta V \delta V(t) \rangle$ TCF observed in equilibrium allows us to assess the range of validity of the linear approach for ionic dynamics.

One aspect of these nonequilibrium simulations must be mentioned before making comparisons to the equilibrium results. When the charge on a solute is abrutply changed the difference in solvation energy appears as added thermal energy that produces local and, for finite samples, global temperature changes. This effect was first observed by Rao and Berne[45] in a simulation of charge jumps, $Ne \rightarrow Ne^{+2}$, in ST2 water (the Ne LJ parameters in this simulation were identical to our $S0$ parameters). For this drastic change in the solute's charge, Rao and Berne observed a dramatic local heating of first solvation shell waters to rotational temperatures of ~1200 K. The tightly bound first coordination sphere was observed to retain much of this high thermal excitation for the 0.6 ps duration of their simulation.[45] As illustrated in Fig. 18, we see a similar, although less dramatic, heating in our charge-jump simulations. In this figure we plot temperatures, determined from the average kinetic energy per molecule in a given shell, as a function of time after the charge jump. (Shell definitions are provided in Table IX.) The largest perturbation we have examined is the $S0 \rightarrow S+$ change shown in Fig. 18(A). In this case the kinet-

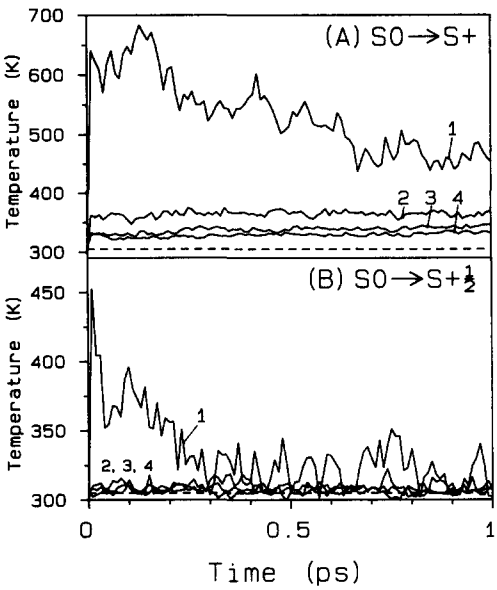

FIG. 18. Temperatures of different solvent regions as a function of time after a charge jump (at $t=0$): (A) $S0\rightarrow S+$ and (B) $S0\rightarrow S+\frac{1}{2}$. Temperatures are based on the total kinetic energy of molecules in a region. The dashed lines indicate the temperature prior to the charge jump. Definitions of the shell regions are provided in Table IX.

ic energy of the ~7 first solvation shell waters increases by an amount equivalent to a 300 K temperature increase. The heating is very rapid, the majority occurring in one librational period. All solvent regions show this abrupt temperature increase, which is presumably communicated from the first shell through the librational/vibrational modes of the hydrogen bonded water network. Relaxation of the majority of the excess first shell energy to the remaining solvent, however, takes place on a much longer time scale of order 1 ps. As a result of the $S0\rightarrow S+$ charge jump, the average total kinetic energy of the 256 cluster rises an amount equal to a 39 K temperature change. With the exception of the reverse ($S+\rightarrow S0$) jump, local heating was much smaller in all of the other nonequilibrium simulations undertaken. The next largest effects were seen with the $S0\rightarrow S+\frac{1}{2}$ case, illustrated in Fig. 18(B). With this smaller charge jump, the kinetic energy rise in the first shell is reduced to the equivalent of ~100 K. By the end of the simulation about 75% of this energy has flowed into the remaining solvent. The overall temperature rise in this case is only ~3–5 K. Jumps of a full electronic charge in the L solutes are similar to the $S0\rightarrow S+\frac{1}{2}$ case in that the overall temperature rise in the sample is again ~3.5 K. The main difference is that, since the number of first solvation shell waters of the L solutes is roughly six times that surrounding $S+\frac{1}{2}$, the initial kinetic energy of temperature change *per molecule* in the first shell is reduced accordingly to ~20 K.

How will this local heating influence the dynamics and comparison to the equilibrium results? First we note that such heating is one feature present in the nonequilibrium situation that might cause departure from linear behavior. We note that finite sample size should not appreciably bias our observation of this effect since the heat dissipation is relatively slow on the solvation time scale. It would be reasonable to assume that local heating would hasten the solvation response. Some idea of the expected magnitude of the change can be obtained by noting that reorientation times determined from NMR measurements[75] decrease by factors of 1.8 and 4.3 as a result of temperature increases of 20 and 80 K, respectively. On this basis, even the fairly modest heating (20 K) of first shell waters produced by a full charge jump in an L solute might be expected to increase the solvation rates noticeably (i.e., twofold) compared to the equilibrium predictions. Via this same reasoning, the ~300 K change in energy of first shell waters in the $S0\rightarrow S+$ simulation would be expected to produce an enormous change in the observed rates. Here, however, the idea of a local temperature is somewhat misleading. Most of the excess energy is tied up in vibrational energy of the strongly bound first shell–solute complex that forms very rapidly upon ionization. We observe that the amplitudes of the translational/vibrational modes such as illustrated in Fig. 17(A) increase while their frequencies remain about the same. This vibrational sort of heating would not be expected to enhance the rate to nearly the extent that an actual temperature change, which serves to speeding up all diffusive motions, does. Thus, while we would expect local heating to have some effect on the $S0\rightarrow S+$ response it should not be as extreme as the 300 K figure might suggest. Finally, we note that the ST2 model does not allow for *intra*molecular vibration of the solvent. The additional heat capacity introduced by such modes should further dampen the effect of local heating in real water compared to what we observe in the simulations.

The results of the charge jump simulations are summarized in Table X and in Figs. 19 and 20. In Fig. 19 we compare the normalized potential response functions $S(t)$ [Eq. (7.1)] for two charge jumps (A) $L0\rightarrow L+$ and (B) $S0\rightarrow S+$ to the $\langle\delta V\delta V(t)\rangle$ TCFs [$C(t)$] observed for these solutes at equilibrium. Consider first the $L0\rightarrow L+$ case shown in Fig. 19(A). At early times, the $S(t)$ response is identical, to within uncertainties, to the $C(t)$ correlation function of the $L0$ solute. At longer times ($t>0.3$ ps) $S(t)$ reaches its ultimate value significantly faster than either of the equilibrium $C(t)$ decays. All four jump simulations in-

TABLE X. Time constants of the nonequilibrium solvation response.

Jump	Nonequilibrium[a] response time	Equilibrium times[b]	
		Initial	Final
$L0\rightarrow L+$	0.07	0.11	0.16
$L0\rightarrow L-$	0.11	0.11	0.21
$L+\frac{1}{2}\rightarrow L+$	0.12	···	0.16
$L+\rightarrow L0$	0.08	0.16	0.11
$S0\rightarrow S\frac{1}{2}$	0.16	0.09	0.20
$S0\rightarrow S+$	0.21	0.09	0.23
$S+\rightarrow S0$	0.04	0.23	0.09

[a] Approximate average response times (ps) of the electrical potential to the indicated charge jumps. These times are integrals of the normalized response functions [Eq. (7.1)] between 0 and 1 ps. Not all responses have decayed to 0 by 1 ps so that the values listed are lower limits to the average time constants.

[b] Approximate average time constants (ps) of the $\langle\delta V\delta V(t)\rangle$ TCFs observed in equilibrium for initial and final states of the jump. Data taken from Table VIII.

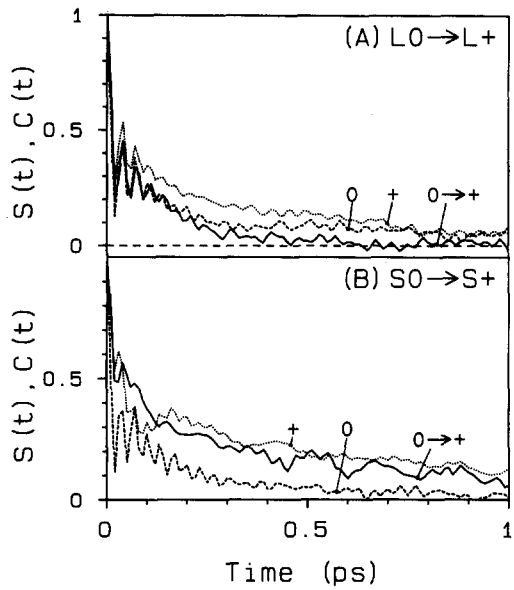

FIG. 19. Response functions of the nonequilibrium potential response to a charge jump [solid curves; $S(t)$ in Eq. (7.1)] compared to $\langle \delta V \delta V(t) \rangle$ TCFs observed in equilibrium at the initial and final states of the jump: (A) $L0 \rightarrow L+$ jump and (B) $S0 \rightarrow S+$ jump.

volving L solutes exhibit this same basic pattern. At short times the $S(t)$ responses are identical to one another and to $C(t)$ of $L0$ at equilibrium. The behavior at longer times can be judged from the approximate time constants listed in Table X. Although the uncertainties in these values are large, (roughly $\pm 30\%$), the $S(t)$ curves for L solutes consistently decay at least as fast, and usually faster than the equilibrium TCFs.

Differences among the S solutes in equilibrium are much larger than among the L solutes so that comparisons to the nonequilibrium simulations are more clear cut. For the $S0 \rightarrow S+$ case illustrated in Fig. 19(B), the nonequilibrium $S(t)$ curve more closely resembles $C(t)$ of the $S+$ solute than that of $S0$. The reproducible maximum at ~ 0.2 ps in $C(t)$ of $S+$ is not found in the $S0 \rightarrow S+$ $S(t)$ decay, however, the decay times are quite similar (Table X). Further, as in the equilibrium $C(t)$ of $S+$, the $S0 \rightarrow S+$ $S(t)$ lacks the pronounced librational oscillations present in the $S0$ TCF.

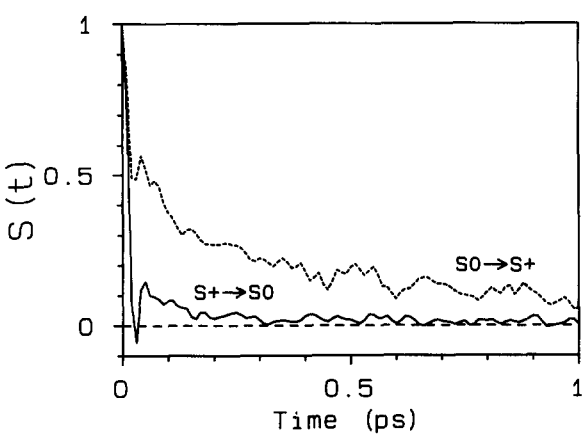

FIG. 20. Comparison of the potential response to the opposite charge jumps $S+ \rightarrow S0$ (solid) and $S0 \rightarrow S+$ (dashed).

In an analogous way the $S0 \rightarrow S+\frac{1}{2}$ response function (not shown) is more similar to the $S+\frac{1}{2}$ equilibrium TCF than to that of $S0$. The average time constants for the $S0 \rightarrow S+\frac{1}{2}$ $[S(t)]$ and $S+\frac{1}{2}$ $[C(t)]$ decays are the same to within our estimated uncertainties.

The response observed with the $S+ \rightarrow S0$ charge jump was unique among the simulations we have performed. Its $S(t)$ curve is shown in comparison to that of the reverse jump ($S0 \rightarrow S+$) in Fig. 20. Whereas all other $S(t)$ responses resemble one or other of the equilibrium TCFs, the $S+ \rightarrow S0$ response is much faster than any equilibrium decay. Most of the relaxation is over within one librational period. The mechanism in this case involves first solvation shell waters undergoing an impulsive reorientation and translation away from the solute. The reason is that the coordination sphere of the initial $S+$ solute is so tightly bound that there is considerable repulsion between neighboring waters, which have further unfavorable LJ interactions with the solute. When the charge is switched off this repulsion is bared and causes very rapid expansion of these waters. None of the other situations investigated has such a switching on of repulsive forces to nearly the same degree as the $S+ \rightarrow S0$ case.

A number of conclusions can be drawn from the above results. First of all, jump of a full electronic charge in either the L or the S solutes cannot *strictly* be described in terms of a linear response. This fact was already apparent from the equilibrium simulations in which we observed that the equilibrium TCFs of $S0$ and $S+$, and even of $L0$, $L+$, and $L-$ were perceptably different. However, in a practical sense we could categorize the behavior of the L solutes with respect to a full charge jump as "nearly linear." Differences among the TCFs of the different L solutes in equilibrium are not large. The charged solutes do decay more slowly at long times but the early time behavior [where most of the $C(t)$ decay occurs] is quite similar in all cases. Furthermore, in the nonequilibrium simulations we actually observe *no* difference between the responses to the opposite charge jumps $L0 \rightarrow L+$ and $L+ \rightarrow L0$, and the differences among the other L solutes do not exceed our uncertainties. Finally, all nonequilibrium response functions closely resemble the equilibrium TCFs, especially that of $L0$. The main difference is again in the long time behavior where the nonequilibrium response appears to be more rapid. We speculate that this slightly faster response is an effect of the local heating discussed earlier. The behavior of the S solutes is more complicated. We would not expect the solvent response to a full electronic charge jump in the S solutes to be well described by a linear response approach. The solvation structures of the $S0$ and $S+$ solutes are very dissimilar, as are their equilibrium dynamics. The dramatic difference between jumps in the $S0 \rightarrow S+$ and $S+ \rightarrow S0$ directions upholds this expectation. Even here, however, the linear response formalism still seems to have some predictive value. Examination of all of the nonequilibrium results (Table X) shows that the linear response prediction *based on the final state* of the solute yields an estimate of the response time correct to within about a factor of 2. This estimate appears to form an upper bound to the observed response time, possibly because of

local heating effects. With the exception of the somewhat pathological $S+ \rightarrow S0$ jump, the shapes of the $S(t)$ curves are also reasonably well predicted by the linear response $C(t)$ of the final state.

VIII. SUMMARY AND CONCLUSIONS

We have used molecular dynamics computer simulations to study the dynamical aspects of solvation of simple spherical solutes in ST2 water. Although we employ solvent clusters in these simulations, we have shown that for the size clusters employed, we are observing behavior characteristic of the bulk solvent. Some sample size effects are noticeable in the dynamical results, however, our qualitative conclusions should be independent of such effects. We now summarize our main results.

The equilibrium simulations yield the time correlation functions $\langle \delta V \delta V(t) \rangle$, $\langle \delta E_z \delta E_z(t) \rangle$, and $\langle \delta V_{zz} \delta V_{zz}(t) \rangle$, whose time dependences are those of the solvation responses to small step function changes in the charge, dipole, and quadrupole moment of a solute. From these simulations we observe the following:

(i) All of the TCFs show a very rapid ($\sim$25 fs) librational decay accounting for roughly half of the total relaxation. The remainder occurs more slowly, on the time scale of tenths of picoseconds.

(ii) The relative rates of decay of the three TCFs follow the order: $\langle \delta V \delta V(t) \rangle > \langle \delta V_{zz} \delta V_{zz}(t) \rangle > \langle \delta E_z \delta E_z(t) \rangle$ for all solutes except $S+$. In all cases the V_{zz} and E_z TCFs are more similar to one another than they are to $\langle \delta V \delta V(t) \rangle$. With the exception of the small charged solutes $S+\frac{1}{2}$ and $S+$, the $\langle \delta V \delta V(t) \rangle$ TCFs exhibit pronounced oscillatory structure due to a collective librational motion of first shell waters. Such oscillations are absent or greatly suppressed in the $\langle \delta E_z \delta E_z(t) \rangle$ and $\langle \delta V_z \delta V_{zz}(t) \rangle$ TCFs.

(iii) Different solutes have different solvation times. All of the large solutes show rather similar behavior, however, at long times solvation of the uncharged ($L0$) solute seems to proceed more rapidly than in the charged ($L+$ and $L-$) solutes. Differences in dynamics are much more pronounced for the small solutes, for which the rate of solvation decreases as the solute charge is increased in the series $S0$, $S+\frac{1}{2}$, $S+$.

(iv) The solvation TCFs observed for the $S0$ and $L0$ solutes are indistinguishable to within our uncertainties. Since these solutes differ in size by a factor of 2.25, solute size does not appear to be of primary importance in this range.

(v) The solvation TCFs decay much more rapidly than any related single molecule TCFs. It is the intermolecular correlations among molecules that cause rapid decay of these equilibrium TCFs, or alternatively, it is the cooperativity of the solvation response that makes it so rapid. For $\langle \delta V \delta V(t) \rangle$ on the order of 10–40 molecules appear to be sufficient to achieve the ultimate response time.

(vi) For the solutes studied, the first solvation shell dominates the response, especially at short times. The relative contributions of librational/reorientational vs vibrational/translational types of motions in the first shell response to a large extent determine the shape and average time constant of the various TCFs. Translational mechanisms of relaxation appear to increase in relative importance as the range of the interaction becomes shorter and, for the S solutes, as the charge is increased.

Comparison of the response to a charge jump measured in nonequilibrium simulations to the corresponding TCF, $\langle \delta V \delta V(t) \rangle$, observed in equilibrium allow for the following conclusions concerning the linearity of the solvation response.

(vii) Abrupt change of a full electronic charge in both the L and the S solutes leads to a local heating of nearby water molecules that dissipates relatively slowly on the solvation time scale. Even for the L solutes, for which local heating of first solvation shell waters involves a temperature change of only $\sim$20 K, this effect would be expected to significantly enhance the rate relative to the constant temperature case.

(viii) All charge jumps involving L solutes produce very similar response functions, which also closely resemble $\langle \delta V \delta V(t) \rangle$ observed for $L0$ in equilibrium. The nonequilibrium response appears to be slightly faster than the equilibrium TCF at long times. Thus a full charge jump in an L solute can be considered "linear enough" for most purposes.

(ix) Jump of a full electronic charge in an S solute is clearly nonlinear as witnessed by the very different relaxation times for the processes $S0 \rightarrow S+$ and $S+ \rightarrow S0$. Even for these cases, we note that predictions based on a linear response calculation from the final state of the charge jump provide estimates of the actual dynamics correct to within a factor of 2.

At this point it is worth mentioning the work of Karim *et al.*[46] who recently performed nonequilibrium simulations very similar to ours. These authors studied the response to step function changes in dipole moment of a spherical solute using the TIPS4P[30,76] model of water. Preliminary results of this work indicate that changes of dipole moment of the order of 8 D may also lead to nonlinear behavior of the kind observed here with unit charge jumps.

We now consider our simulation results in light of experimental measurements of solvation rates. Due to limitations of experimental time resolution it is appropriate to use the long-time component of the simulated response for this comparison. Based on the experimental correlation between τ_{solv}/τ_L and $\epsilon_0/\epsilon_\infty$ observed in a variety of solvents[21,22] we would anticipate the solvation response in ST2 water to decay with a time constant of $\sim$9 ps (at long times). The simulated results are in clear disagreement with such an estimate.[77] None of the solutes studied exhibit such a long component in any of their responses. Rather, our results would indicate that water does not obey the same correlation found with other solvents. At long times, the solvation energy relaxes with a time constant in the range $\sim$1–3 τ_{L1}, or $\sim$0.5–1.5 ps, for most solutes. Having made this comparison, it is worth pointing out that the present results are for the ST2 water *model* of water and not for real water itself. We cannot rule out the possibility that features of experimental solvents not included in this model, such as vibrational and electronic polarizability, may substantially alter the time scales of solvation. For the present however, the

similarity between the longitudinal relaxation times of the ST2 model and real water encourages us to conjecture that the solvation times observed here are representative of the experimental solvent as well. Time-resolved Stokes shift measurements of solvation in water have not yet been made but are currently underway[79] and should provide an important test of this prediction. We note that related measurements involving electron solvation in water have recently been reported by Migus *et al.*[80] These workers observed the absorption spectrum characteristic of the fully hydrated electron to arise with a time constant of 0.24 ps. This value, while in reasonable agreement with the times observed here, must be viewed with caution. Changes in the solvated electron spectrum seem to reflect a change in electronic state during solvation rather than simply a continuous relaxation of the solvent surroundings[80] as in our simulations or in experiments with other probes. Interpretation of the electron solvation time is thus uncertain.

Finally, we compare the behavior observed in our simulations to current theoretical ideas of the solvation response. In Sec. VI we showed that neither the simple continuum model nor the best presently available molecular model can account quantitatively for the simulated results. Here we want to consider how well the qualitative features of our data compare to expectations. It is generally accepted that the solvation response time predicted from simple continuum models (i.e., τ_L in Debye solvents) should provide a lower limit to the actual solvation time scale. If we ignore the $S + \rightarrow S0$ case, we do not observe response times significantly faster than the continuum prediction. In many cases, however, the times we do observe are very close to the continuum prediction, and are much faster than predicted by the molecular, MSA theory. The reason for the disagreement appears to be due to the fast response contributed by first solvation shell waters. As discussed in Sec. I, deviations from simple continuum behavior are usually thought of as resulting from a variation of the response times of the solvent with distance from the solute. Solvent nearest the solute is pictured as having a relatively slow response, and only far from the solvent does the limiting, continuum time scale pertain. We do observe that correlation functions of the radial shell polarizations [Fig. 14(B)] decay most slowly near to the solute. However, the potential TCF of the first shell is actually *faster* than that of the other shells [Fig. 14(A)], which decay similarly to their respective polarization TCFs. Thus the solvation response, measured by $\langle \delta V \delta V(t) \rangle$, is sensitive to factors not taken into account by the shell polarization alone. The fact that the solute senses the full charge distribution of nearby solvent molecules, rather than seeing them as simply point dipoles, changes the dynamics, in this case making it faster.[81]

The importance of the first shell response as well as its complex character is perhaps the most important result of our study. Effects due to the extended charge distribution of the solvent, and translational modes of relaxation become important at close range. Such effects are not represented in the measured $\epsilon(\omega)$, nor are they included in any presently available molecular model. Not only do these effects change the quantitative result, they also cause disagreement with the qualitative picture of a slow nearest-neighbor response.

All current theories of solvation dynamics assume that the solvent responds linearly to changes in the solute. In Sec. IV we observed that the equilibrium solvation energies were linear with respect to changes in solute charge over a wide range of charge/size ratios. With respect to dynamics, we observe that although a unit charge jump cannot strictly be described by a linear response, in most cases the linear approximation provides a reasonable representation of the actual response.

We conclude by observing that for a theoretical model to adequately describe the dynamics of solvation in water, a much more sophisticated treatment of the solvation structure seems necessary. Nonlinear effects, while present, are less important than is properly accounting for the detailed nature of the first solvation shell interactions which lead to the dynamic differences observed with different solutes and responses. A model sufficient to accurately predict the effects we observe would likely be too complex to be instructive. Water is one of the most highly structured of solvents and so its dynamics are probably more complex and solute specific than other polar solvents. However, the importance of the extended charge distribution of solvent molecules and translational mechanisms of relaxation observed for water should pertain to other solvents as well. Thus, development of simple theoretical models capable of treating such effects would be of interest. So too would further simulations using simpler model solvents. We are currently beginning such simulations with a model acetonitrile solvent.

ACKNOWLEDGMENTS

The work reported here was supported by grants from the National Science Foundation. We also acknowledge generous allocations of computer time at the National Center for Supercomputing Applications under Grant No. CHE8303997. During the course of this work we have benefited from numerous discussions with Peter Wolynes, Casey Hynes, Paul Barbara, John Simon, Biman Bagchi, and Ed Castner. We would also like to thank Stuart Rice and Michael Townsend providing us computer code for the ST2 interaction potential, and Martin Neumann for sharing results of his determination of $\epsilon(\omega)$ of ST2 water prior to publication.

APPENDIX: ESTIMATION OF THE DIELECTRIC PROPERTIES OF ST2 WATER

In order to compare our solvation dynamics results to theoretical predictions, the dielectric dispersion $\epsilon(\omega)$ of the solvent is needed as input. Since this was not known for the ST2 model we made a preliminary determination based on pure cluster simulations. Neumann[61] is now in the process of making a more accurate determination of $\epsilon(\omega)$ and although we employ his results in Sec. VI, we present our cluster calculations here for the sake of comparison.

The method we employ is due to Bossis and coworkers.[82,83] The static dielectric constant is obtained via simulation of a generalized, radially dependent Kirkwood g factor $G(r/R)$ for a spherical sample of radius R. $G(r/R)$ is defined by

$$G(r/R) = \left\langle \frac{\mathbf{M}^2(r)}{\mu^2 n(r)} \right\rangle, \tag{A1}$$

where $n(r)$ and $\mathbf{M}(r)$ are the number of molecules and total moment of a (centered) spherical region of radius r and μ is the molecular dipole moment. This quantity is related to the dielectric constant ϵ_0 by[82,83]:

$$G(r/R) = \frac{1}{y}\frac{(\epsilon_0 - 1)}{9\epsilon_0(\epsilon_0 + 2)} \times \left\{ (\epsilon_0 + 2)(2\epsilon_0 + 1) - 2(\epsilon_0 - 1)^2 \left(\frac{r}{R}\right)^3 \right\} \tag{A2}$$

with

$$y = \frac{4\pi\rho\mu^2}{9kT}.$$

Relations (A1) and (A2) are derived for macroscopic samples. In order to apply the relation to microscopic clusters Eq. (A1) must be replaced by[82]:

$$G(r/R) = \left\langle \frac{\mathbf{M}(r - r_c)\cdot\mathbf{M}(\mathbf{r})}{\mu^2 n(r - r_c)} \right\rangle, \tag{A3}$$

where r_c is a length on the order of a few molecular diameters over which dipolar orientations are strongly correlated. Plotting $G(r/R)$ obtained from simulated $\mathbf{M}(r)$ data according to Eq. (A3) vs $(r/R)^3$ should yield a straight line whose slope gives ϵ_0.

Figure 21 shows the results of such a calculation of ϵ_0 using a simulation of a cluster of 512 molecules at 291 K. The simulation was run for a total of 250 ps using a step size of 5 fs. The cluster radius R was taken to be 4.97σ, which is the radius the sample would have if the density profile were a step function. The correlation length r_c was chosen to be 2σ. Error bars in this figure reflect the statistical uncertainty due to limited simulation length. The solid lines are the behavior expected based on Eq. (A2) for two values of ϵ_0 that bracket the statistical error range. To within the statistical uncertainties, the simulated data are adequately represented by an $(r/R)^3$ dependence except near to the cluster boundary. (In this region the error bars are approximately the size of the data points.) Based on the range of the statistical error alone, a value of $\epsilon_0 = 340 \pm 90$ is obtained. The actual error is likely to be greater than this due to the relatively small size of the cluster used. This makes the calculation sensitive to the choices of R and r_c as well as possible effects due to preferential surface orientation of molecules. For these reasons we estimate the static dielectric constant of ST2 water to be 340 ± 150 at 291 K. Even with such wide error limits it is clear that the ST2 model grossly overestimates the dielectric constant of water.

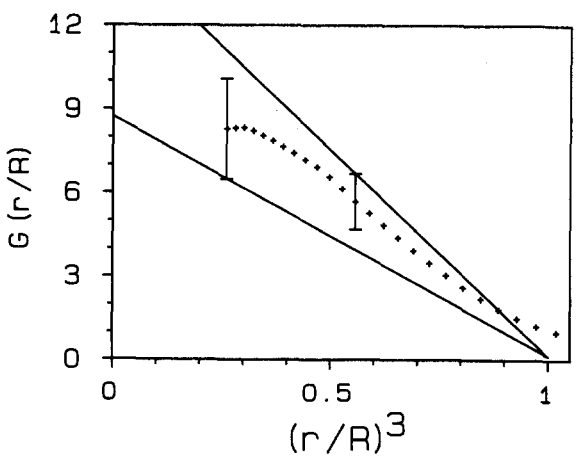

FIG. 21. Generalized Kirkwood g factor $G(r/R)$; Eq. (A3) observed in a 250 ps simulation of a pure 512 cluster. The error bars show the statistical uncertainty due to finite simulation length. The solid lines show the range of linear fits to Eq. (A2) consistent with this uncertainty. The two lines correspond to $\epsilon_0 = 253$ (upper) and $\epsilon_0 = 432$ (lower).

The frequency dependence of the dielectric response can be estimated from the same simulation from the time correlation function of the total dipole moment of the cluster $\langle \mathbf{M}\cdot\mathbf{M}(t)\rangle$. $\epsilon(\omega)$ is related to the normalized TCF $\Phi(t)$,

$$\Phi(t) = \langle \mathbf{M}\cdot\mathbf{M}(t)\rangle / \langle M^2 \rangle \tag{A4}$$

by

$$\left(\frac{\epsilon(\omega) - 1}{\epsilon(\omega) + 2}\right)\left(\frac{\epsilon_0 + 2}{\epsilon_0 - 1}\right) = \mathcal{L}_{i\omega}\left\{ -\frac{d\Phi}{dt} \right\}, \tag{A5}$$

where $\mathcal{L}_{i\omega}$ denotes a Laplace transform. Figure 22 shows the $\Phi(t)$ obtained from the simulation described above. The error bar shown on the graph is again the estimated statistical uncertainty in the averaging. $\Phi(t)$ can be represented by a sum of two exponentials as

$$\Phi(t) = fe^{-t/\tau_1} + (1 - f)e^{-t/\tau_2} \tag{A6}$$

with values $f = 0.72$, $\tau_1 = 0.76$ ps, and $\tau_2 \sim 0.012$ ps. This result is independent of the value of ϵ_0. We obtained parameters describing the $\epsilon(\omega)$ function by performing the Laplace transform in Eq. (A5) on this fitted $\Phi(t)$. The resultant dielectric dispersion can be represented by a sum of two Debye processes with the constants

$$\epsilon_{01} = \epsilon_0 = 340, \quad \tau_{D1} = 64 \text{ ps},$$
$$\epsilon_{\infty 1} = \epsilon_{02} = 2.1, \quad \tau_{D2} = 0.016 \text{ ps},$$
$$\epsilon_{\infty 2} = \epsilon_\infty = 1.$$

It is instructive to compare these cluster results to those obtained by Neumann[61] using a periodic simulation. (The later results are provided in Sec. VI.) The dielectric constant

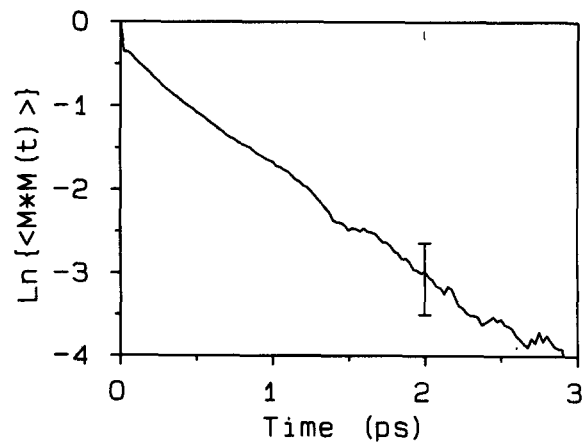

FIG. 22. Correlation function of the total dipole moment [Eq. (A4)] of a pure 512 cluster.

that we obtain is considerably higher than Neumann's value of 218, however, they are consistent to within the estimated error limits. The values of τ_{D1} differ by a factor of 2 between the two determinations but this is simply a reflection of the difference in ϵ_0. The long-time part of $\Phi(t)$ decays on a time scale that is approximately proportional to τ_{D1}/ϵ_0. Error in ϵ_0 then appears as a proportional error in τ_{D1} in cluster simulations. (This is not true of bulk simulations.) Rather than comparing the $\epsilon(\omega)$ parameters derived by the two simulations, the more relevant comparison as far as solvation dynamics is concerned is to compare the time dependence of $\Phi(t)$. $\Phi(t)$ decays in a manner closely related to the decay of longitudinal dielectric fluctuations which, in the continuum limit, determine solvation dynamics. Using the inverse of Eq. (A5), Neumann's $\epsilon(\omega)$ results can be transformed into a $\Phi(t)$ to compare to the function measured directly here. Treating Neumann's $\epsilon(\omega)$ in this manner yields a $\Phi(t)$ decay that agrees with our result to well within our estimated error. This agreement between our results and the bulk simulations of Neumann is noteworthy. It indicates that the presence of the cluster surface, while it may influence determination of ϵ_0 and $\epsilon(\omega)$, should not appreciably affect the solvation dynamics of most interest to us here.

[1]See, for example, the papers in Faraday Discuss. Chem. Soc. **85** (1988) for a survey of current areas of research.

[2]D. F. Calef and P. G. Wolynes, J. Phys. Chem. **87**, 3387 (1983); J. Chem. Phys. **78**, 470 (1983).

[3]H. Sumi and R. A. Marcus, J. Chem. Phys. **84**, 4894 (1986); W. Nadler and R. A. Marcus, *ibid.* **86**, 3906 (1987).

[4]J. P. Bergsma, B. J. Gertner, K. R. Wilson, and J. T. Hynes, J. Chem. Phys. **86**, 1356 (1987); B. J. Gertner, J. P. Bergsma, K. R. Wilson, S. Lee, and J. T. Hynes, *ibid.* **86**, 1377 (1987).

[5]I. Rips and J. Jortner, J. Chem. Phys. **87**, 2090 (1987).

[6]D. A. Zichi and J. T. Hynes, J. Chem. Phys. **88**, 2513 (1988).

[7]M. Sparpaglione and S. Mukamel, J. Chem. Phys. **88**, 3263 (1988).

[8]T. Mazurenko Yu, Opt. Spectrosc. (USSR) **36**, 283 (1974).

[9]B. Bagchi, D. W. Oxtoby, and G. R. Fleming, Chem. Phys. **86**, 257 (1984).

[10]G. van der Zwan and J. T. Hynes, J. Phys. Chem. **89**, 4181 (1985).

[11]R. F. Loring, Y. J. Yan, and S. Mukamel, Chem. Phys. Lett. **135** (1987).

[12]E. W. Castner, Jr., B. Bagchi, and G. R. Fleming, Chem. Phys. Lett. **143**, 270 (1988).

[13]The influence of nonspherical shapes has recently been considered by Castner *et al.* in Ref. 12.

[14]Homogeneous continuum models predict slightly different time constants for the solvation response to step function changes in different multipole moments; however, in most cases, all times are within ~20% of τ_L (see Ref. 22).

[15]E. W. Castner, Jr., M. Maroncelli, and G. R. Fleming, J. Chem. Phys. **86**, 1090 (1987).

[16]M. Maroncelli and G. R. Fleming, J. Chem. Phys. **86**, 6221 (1987).

[17]E. W. Castner, Jr., B. Bagchi, M. Maroncelli, S. P. Webb, A. J. Ruggiero, and G. R. Fleming, Ber. Bunsenges. Phys. Chem. **92**, 363 (1988).

[18]V. Nagarajan, A. M. Brearley, T.-J. King, and P. F. Barbara, J. Chem. Phys. **86**, 3183 (1987).

[19]M. A. Kahlow, T.-J. Kang, and P. F. Barbara, J. Chem. Phys. **88**, 2372 (1988).

[20]S.-G. Su and J. D. Simon, J. Phys. Chem. **91**, 2693 (1987); J. D. Simon and S.-G. Su, J. Chem. Phys. **87**, 7016 (1987).

[21]M. Maroncelli and G. R. Fleming, J. Chem. Phys. **89**, 875 (1988).

[22]E. W. Castner, Jr., G. R. Fleming, B. Bagchi, and M. Maroncelli, J. Chem. Phys. (in press).

[23]D. F. Calef and P. G. Wolynes, J. Chem. Phys. **78**, 4145 (1983).

[24]R. F. Loring and S. Mukamel, J. Chem. Phys. **87**, 1272 (1987). See also R. F. Loring, Y. J. Yan, and S. Mukamel, *ibid.* **87**, 5840 (1987).

[25]V. Friedrich and D. Kivelson, J. Chem. Phys. **86**, 6425 (1987).

[26]P. G. Wolynes, J. Chem. Phys. **86**, 5133 (1987).

[27](a) I. Rips, J. Klafter, and J. Jortner, J. Chem. Phys. **88**, 3246 (1988); (b) J. Chem. Phys. (in press).

[28]A. L. Nichols III and D. F. Calef, J. Chem. Phys. **89**, 3783 (1988).

[29]F. H. Stillinger and A. Rahman, J. Chem. Phys. **60**, 1545 (1974).

[30]W. L. Jorgensen, J. Chandrasekhar, J. D. Madura, R. W. Impey, and M. L. Klein, J. Chem. Phys. **79**, 926 (1983).

[31]See, for example, the series *Water a Comprehensive Treatise*, edited by F. Franks (Plenum, New York, 1972–1979), Vols. 1–6.

[32]A. Geiger, A. Rahman, and F. H. Stillinger, J. Chem. Phys. **70**, 263 (1979); C. Pangali, M. Rao, and B. J. Berne, *ibid.* **71**, 2975 (1979).

[33]A recent review is K. Heinzinger and G. Palinkas, in *The Chemical Physics of Solvation*, edited by R. R. Dogonadze *et al.* (Elsevier, Amsterdam, 1985), Part A, p. 313.

[34]K. Nakananishi, K. Ikari, S. Okazaki, and H. Touhara, J. Chem. Phys. **80**, 1656 (1984).

[35]K. Remerie, J. B. F. N. Engberts, and W. F. van Gunsteren, Chem. Phys. **101**, 27 (1986).

[36]J. Schnitker and P. J. Rossky, J. Chem. Phys. **8**, 3471 (1987).

[37]A. Wallqvist, G. Martyna, and B. J. Berne, J. Phys. Chem. **92**, 1721 (1988).

[38]A. Geiger, Ber. Bunsenges. Phys. Chem. **85**, 52 (1983).

[39]Gy. I. Szasz and K. Heinzinger, J. Chem. Phys. **79**, 3467 (1983).

[40]D. A. Zichi and P. J. Rossky, J. Chem. Phys. **84**, 2814 (1986).

[41]H. L. Nguyen and S. A. Adelman, J. Chem. Phys. **81**, 4564 (1984).

[42]M. A. Wilson, A. Pohorille, and L. Pratt, J. Chem. Phys. **83**, 5832 (1985).

[43]M. Merkowitz and W. Wan, J. Chem. Phys. **86**, 376 (1987).

[44]S. Engström, B. Jönsson, and R. W. Impey, J. Chem. Phys. **80**, 5481 (1984); S. Engström, B. Jönsson, and B. Jönsson, J. Magn. Reson. **50**, 1 (1982).

[45]M. Rao and B. J. Berne, J. Phys. Chem. **85**, 1498 (1981).

[46]O. A. Karim, A. D. J. Haymet, M. J. Banet, and J. D. Simon, J. Phys. Chem. **91**, 3391 (1988).

[47]The notation we employ here is similar to the formulation of W. Bernard and H. B. Callen, Rev. Mod. Phys. **31**, 1017 (1959).

[48]J. A. Barker and R. O. Watts, Mol. Phys. **26**, 789 (1973).

[49]V. M. Jansoone, Chem. Phys. **3**, 78 (1974).

[50]See the recent review by S. W. deLeeuw, J. W. Perram, and E. R. Smith, Annu. Rev. Phys. Chem. **37**, 245 (1986); and C. G. Gray, Y. S. Sainger, C. G. Joslin, P. T. Cummings, and S. Goldman, J. Chem. Phys. **85**, 1502 (1986) for current perspectives on this topic. The continuum description of M. Neumann and O. Steinhauser, Mol. Phys. **39**, 437 (1980) is also helpful in understanding the origin of artifacts observed in early simulations.

[51]It is worth pointing out that the use of periodic boundary conditions does not eliminate the need for large sample sizes. For example, in the Ewald summation method the long-range interactions between molecules in the central simulation cell and molecules in an infinite periodic array of replica cells are accounted for exactly via a lattice summation. If one is concerned about solvation of a single ion, the periodicity imposes artifacts near the cell boundaries analogous to those in a cluster. Thus, as one crosses the boundary from the central cell to a replica cell, the polarization of the solvent reverses sign in an unphysical way. The error incurred via this effect may in fact be worse than that obtained using free clusters. Only with sufficiently large samples does this effect become negligible.

[52]L. Verlet, Phys. Rev. **159**, 98 (1967).

[53]J.-P. Ryckaert, G. Ciccotti, and H. J. C. Berendsen, J. Comput. Phys. **23**, 327 (1977).

[54]H. C. Andersen, J. Comput. Phys. **52**, 24 (1983).

[55]R. M. Townsend, J. Gryko, and S. A. Rice, J. Chem. Phys. **82**, 4391 (1985).

[56]J. G. Powles, J. Chem. Phys. **21**, 633 (1953).

[57]U. Kaatze and V. Uhlendorf, Z. Phys. Chem. N. F. **126**, 151 (1981).

[58]M. R. Mruzik, Chem. Phys. Lett. **48**, 171 (1977).

[59]E. N. Brodskaya and A. I. Rusanov, Mol. Phys. **62**, 251 (1987).

[60]A. P. Shreve, J. P. R. B. Walton, and K. E. Gubbins, J. Chem. Phys. **85**, 2178 (1986).

[61]M. Neumann (private communication).

[62]D. Y. C. Chan, D. J. Mitchell, and B. W. Ninham, J. Chem. Phys. **70**, 2946 (1979).

[63]See, for example, C. G. Gray and K. E. Gubbins, *Theory of Molecular*

Fluids (Oxford, New York, 1984), Vol. 1, Chap. 5.
[64]G. Engel and H. G. Hertz, Ber. Bunsenges. Phys. Chem. **72**, 808 (1968).
[65]Experimentally the librational motion in liquid water gives rise to a broad band at $\sim 600\ cm^{-1}$ in the IR spectrum (Ref. 66), in approximate agreement with the time scale observed for the ST2 model.
[66]See, for example, D. Eisenberg and W. Kauzmann, *The Structure and Properties of Water* (Oxford, New York, 1969), Sect. 4.7.
[67]Apparently similar librational oscillations were observed in the decay of the longitudinal dipole moment correlation function of MCY water by R. W. Impey, P. A. Madden, and I. R. McDonald, Mol. Phys. **46**, 513 (1982).
[68]The force autocorrelation functions determined in Ref. 4 and especially in Refs. 42 and 44 are closely related to $\langle \delta E_z \delta E_z(t) \rangle$ TCFs determined here. Unfortunately, these force autocorrelation functions include forces due to van der Waals interactions in addition to electrostatic forces and so are not directly comparable.
[69]O. Matsuoka, E. Clementi, and M. Yoshimine, J. Chem. Phys. **64**, 1351 (1976); G. C. Lie, E. Clementi, and Y. Yoshimine, *ibid.* **64**, 2314 (1976).
[70]M. Neumann, J. Chem. Phys. **82**, 5663 (1985).
[71]Actually, a more appropriate comparison to the experimental τ_L is with the long-time decay of the continuum prediction for $S(t)$ of an ion [Fig. 12(B)]. This time constant is 0.49 ps, slightly longer than τ_{L1} due to the effect of the second dispersion region.
[72]Nichols and Calef (Ref. 28) have, however, obtained a solution for arbitrary solute size of a single Debye $\epsilon(\omega)$.
[73]We have calculated the single-molecule contribution to $\langle \delta V \delta V(t) \rangle$ in a few cases but do not show the results here because of poor signal to noise.
[74]These two types of intramolecular motions have vibrational character at short times and are what give rise to librational and hindered translational modes observed in the IR and Raman spectra of liquid water (Ref. 66).
[75]J. Jonas, T. DeFries, and D. J. Wilbur, J. Chem. Phys. **65**, 582 (1976).
[76]W. L. Jorgensen and J. D. Madura, Mol. Phys. **56**, 1381 (1985).
[77]In a preliminary communication of the work presented here (Ref. 78), we concluded that the simulation results were consistent with the experimental estimate. This erroneous conclusion was due to poor estimates of the longitudinal relaxation time and dielectric constant of ST2 water.
[78]M. Maroncelli, E. W. Castner, Jr., S. P. Webb, and G. R. Fleming, in *Ultrafast Phenomena V*, edited by G. R. Fleming and A. E. Siegman (Springer, Heidelberg, 1986), p. 303.
[79]A. Ruggiero, S. J. Rosenthal, L. Dhar, and G. R. Fleming (in preparation).
[80]A. Migus, Y. Gaudel, J. L. Martin, and A. Antonetti, Phys. Rev. Lett. **58**, 1559 (1987).
[81]Although not shown, we see the same differences between the shell polarizations and the potentials in the nonequilibrium simulations that we do in the equilibrium case.
[82]C. Hesse-Bezot, G. Bossis, and C. Brot, J. Chem. Phys. **80**, 3399 (1984); G. Bossis, Mol. Phys. **38**, 2023 (1979).
[83]See also J. G. Powles and R. F. Fowler, J. Phys. C **18**, 5909 (1985); J. G. Powles, R. F. Fowler, and W. A. B. Evans, Chem. Phys. Lett. **107**, 280 (1984).